International Journal of Speleology	53 (2)	89-110	Tampa, FL (USA)	June 2024

Available online at scholarcommons.usf.edu/ijs

International Journal of Speleology

Official Journal of Union Internationale de Spéléologie

A speleogenetic history of Novoafonskaya Cave in the Western Caucasus

Olga Y. Chervyatsova [1], Sergey S. Potapov [2], Jonathan L. Baker [3], Dmitry A. Gavryushkin [4], Victor J. Polyak [5], Matt Heizler[6], Sergey V. Tokarev [7], Sergey A. Sadykov [2], Roman S. Dbar [8], and Yuri V. Dublyansky [3]

[1]Shulgan-Tash State Natural Biosphere Reserve, Zapovednaya 14, Irgyzly, Burzyan District, Bashkortostan Republic, 453585, Russia
[2]South Urals Research Center of Mineralogy and Geoecology, Ural Branch of the Russian Academy of Sciences, Miass, 456317, Russia
[3]Institute of Geology, Innsbruck University, Innrain 52, Innsbruck, 6020, Austria
[4]Schmidt Institute of Physics of the Earth of the Russian Academy of Sciences, Bolshaya Gruzinskaya str. 10/1, Moscow, 123242, Russia
[5]Radiogenic Isotope Laboratory, 221 Yale Blvd, Northrop Hall, University of New Mexico, Albuquerque, New Mexico 87131, USA
[6]New Mexico Geochronology Research Laboratory, New Mexico Tech, 801 Leroy Place, Socorro, NM 87801, USA
[7]V.I. Vernadsky Crimean Federal University, Prospekt Vernadskogo 4, Simferopol, 295007, Crimea
[8]Institute of Ecology, Academy of Sciences of Abkhazia, Krasnomayatskaya str. 67, Sukhum, 384900, Abkhazia

Abstract: Speleogenesis in hypogene karst settings may be closely tied to regional tectonic dynamics and concomitant hydrochemical evolution of karst waters. However, placing temporal constraints on these processes can require a wider array of field observations and techniques than for typical karst systems. Herein, we present a comprehensive study of Novoafonskaya Cave (Western Caucasus, Abkhazia). The updated speleogenetic history of the cave comprises four stages: (1) the most ancient, a low-T hydrothermal (ca. 40–50°C) priming stage; (2) the main stage enabled by mixing of upwelling thermomineral and locally recharged common karst waters; (3) the late sulfuric-acid speleogenesis (SAS) stage, which left significant mineralogical overprint (gypsum and a suite of minerals resulting from the alteration of silicate sediments) but did not alter the morphology of the cave appreciably; and (4) the contemporary stage, occurring predominantly in the phreatic and epiphreatic zones. Ages of speleogenetic stages were constrained by radiometric dating (^{230}Th-U and ^{40}Ar/^{39}Ar) and paleomagnetic data, alongside the Quaternary geological history of the region and paleodynamics of the Black Sea level. Conditions for the low-T hydrothermal karstification occurred from Miocene – Middle Pliocene. The main stage, which created the main volumes of the cave, took place from Late Pliocene – Middle Pleistocene. The cave emerged from the phreatic into the vadose zone after ca. 400 ka ago, due to the combined effect of the Black Sea regression and intensification of tectonic uplift in the Caucasus. The presence of sulfidic waters during dewatering led to the development of transient SAS processes during Middle to Late Pleistocene. Dating of calcite underlying SAS-associated overgrowths constrains the cessation of this SAS activity to within the last 147 ka. In its present state, the cave has no connection with thermomineral waters; however, such waters are found deeper in the southern parts of the karst massif (based on the hydrochemistry of Psyrtskha spring), implying that hypogene karstification, primarily driven by mixing corrosion, may still be active deep in the phreatic zone.

Keywords: speleogenesis, hypogene, sulfuric acid speleogenesis, Abkhazia

Received 26 February 2024; Revised 14 May 2024; Accepted 21 May 2024

Citation: Chervyatsova, O.Y., Potapov, S.S., Baker, J.L., Gavryushkin, D.A., Polyak, V.J., Heizler, M., Tokarev, S.V., Sadykov, S.A., Dbar, R.S., Dublyansky, Y.V., 2024. A speleogenetic history of Novoafonskaya Cave in the Western Caucasus. International Journal of Speleology, 53(2), 89-110. https://doi.org/10.5038/1827-806X.53.2.2499

INTRODUCTION

Discovered in the early 1960's, Novoafonskaya Cave (variants: Novy Afon Cave, New Athos Cave, Anakopiyskaya Cave, Akhali Atoni Cave) is located near the Black Sea coast in Abkhazia and remains one of the best-known caves in the region. Early researchers interpreted Novoafonskaya Cave as epigene, and its formation was attributed to the focused discharge of large volumes of flood waters (Tintilozov, 1976). Subsequently, a multistage hypogene-epigene model was proposed by V. Dublyansky (1981), according to which the cave began to form in confined conditions under the influence of thermomineral waters. As the

*kittary@yandex.ru

hydrodynamic opening of the hydrogeologic system progressed, mixing corrosion became the dominant mechanism of karst formation, replaced at later stages by epigene karstification.

Caves with multistage evolution (in which the sources of fluids and types of processes changed as hydrodynamic opening proceeded) are the most difficult for speleogenetic reconstructions, since geomorphological and mineralogical indicators of ancient stages may be partially lost due to later processes of sedimentation, corrosion, collapse, etc. (Columbu et al., 2021). Herein, we propose an updated speleogenetic model of Novoafonskaya Cave that is guided by comprehensive geochemical, mineralogical, and hydrochemical constraints. For the first time, we are able to approximate key chronological boundaries of individual phases through radiometric techniques, in concert with recent studies of the cave and its geological setting. Our interpretations further rely on modern developments in the fields of the morphology, hydrogeology, isotope geochemistry and mineralogy of hypogene speleogenesis (Polyak & Provencio, 2001; Galdenzi & Maruoka, 2003; Klimchouk, 2007; Dublyansky, 2013; D'Angeli et al., 2018, 2019; Audra et al., 2022; Spötl et al., 2021, 2023; De Waele et al., 2024).

DESCRIPTION OF THE STUDY AREA

Geology and physiography

The foremost ridges of the western Caucasus comprise carbonate rocks of Cretaceous and Upper Jurassic age and constitute one of the most important karst regions of the Caucasus. Alpine-type epigene karst is actively developing in the high-mountain massifs. A number of deep caves have been explored here, including the world's four deepest: Veryovkina (depth 2212 m), Krubera (2199 m), Sarma (1830 m), and the Snezhnaya-Mezhennogo-Illyusiya-Banka cave system (1760 m) (Vakhrushev et al., 2001; Gusev, 2018; Klimchouk, 2018; Barashkov et al., 2021). In the discharge zone, confined to the low-lying ridges of the coastal massifs along the Black Sea, horizontal water-bearing cave systems are developed (Tintilozov, 1976; Vakhrushev et al., 2001; Zakharov et al., 2018).

Our study area (Fig. 1a) is located at the junction of the low-altitude (800–1200 m a.s.l.) foremost ridges of the Western Caucasus and the Gudauta coastal lowland west of the Colchis lowland (Ekba & Dbar, 2007). The region has a Mediterranean climate, classified as *Csa* on the coast and *Csb* in the mountainous zone (Köppen-Geiger classification; Peel et al., 2007). Mean annual temperature near the coast is 14.8°C, whereas the minimum and maximum mean monthly temperatures are observed in January (6.0°C) and August (24.3°C), respectively (Ekba & Akhsalba, 2018). Assuming a regional lapse rate of 5–6°C/km (Ekba & Dbar, 2007; Wolf et al., 2024), temperatures in the mountainous part are 5–12°C lower. Mean annual precipitation is 1600 mm along the coast but increases to >2100 mm at altitudes of 500–1000 m and can exceed 3000 mm in the high massifs. About 60% of precipitation falls during the autumn-winter period, when evaporation is minimal (Tintilozov, 1976).

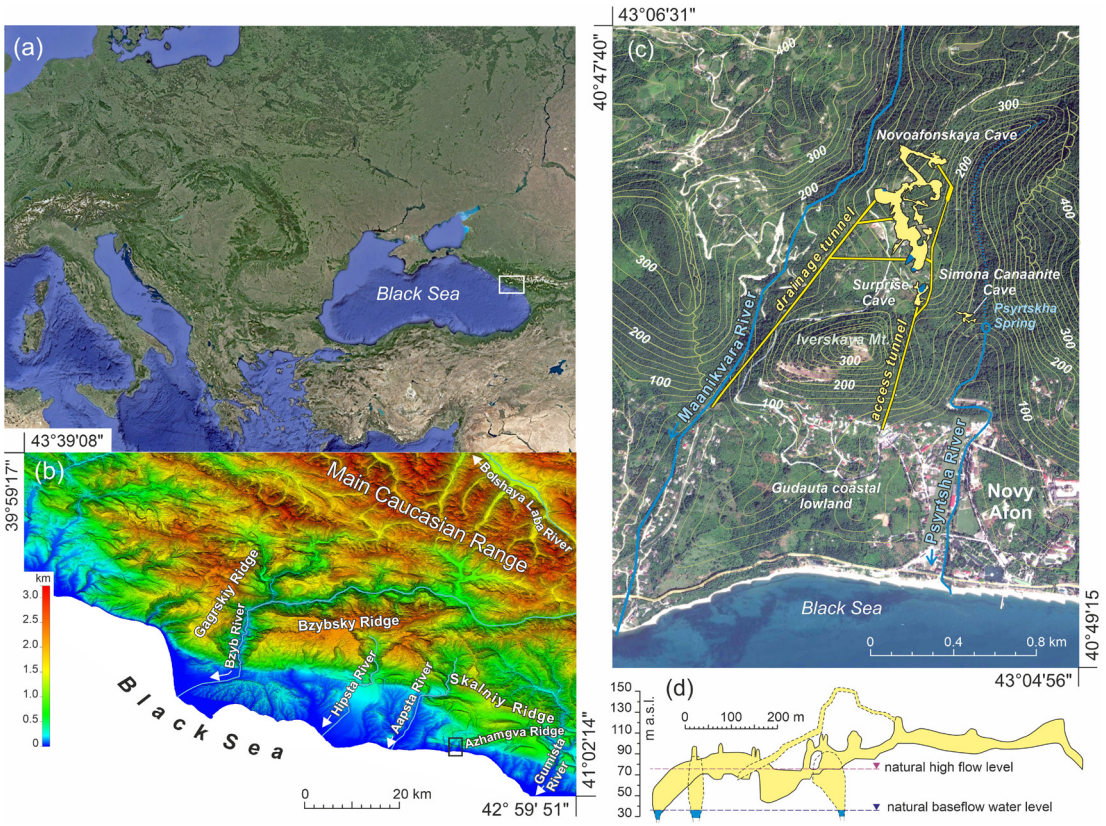

Fig. 1. Study area and geographic context of Novoafonskaya Cave: (a) Overview map; white rectangle corresponds to (b); (b) Position of the cave in relation to the Black Sea and mountain ranges of the western part of Abkhazia (relief according to SRTM30; Smith & Sandwell, 1997). Black rectangle corresponds to (c); (c) Novoafonskaya Cave and tunnels, in context of the relief and hydrological network (overlay on Google Earth image); (d) Schematic cross section of the cave (without natural entrance shaft) and karst water levels.

The area of Novoafonskaya Cave is located on the continuation of the overthrust structures of the southern macro-slope of the Greater Caucasus (Nesmeyanov, 2012; Rogozhin et al., 2014). The cave is located in the hinge part of the Azhamgva anticline, dipping in this area in the NW direction (Fig. 2a-c). The core of the anticline is composed of Lower Cretaceous limestone (Hauterivian-Barremian) up to 500 m thick and is covered by partially denuded Aptian-Albian marls interbedded with clay and siltstone. The southern flank of the anticline exposes Upper Cretaceous rocks represented by clay, sandstone, limestone and marl.

The southern wing of the anticline is cut by a sublatitudinal thrust fault (Rogozhin et al., 2014). South of the fault, blocks of Cretaceous and Paleogene rocks dip to a depth of 0.5–1.5 km under a sequence of low-permeability molasse sediments of Oligocene-Neogene age (Afanasenkov et al., 2007). North of the fault, there are a number of genetically related second-order faults (Fig. 2b, c). One of them with displacement amplitude exceeding 50 m is located between Novoafonskaya and Surprise caves (Fig. 2c).

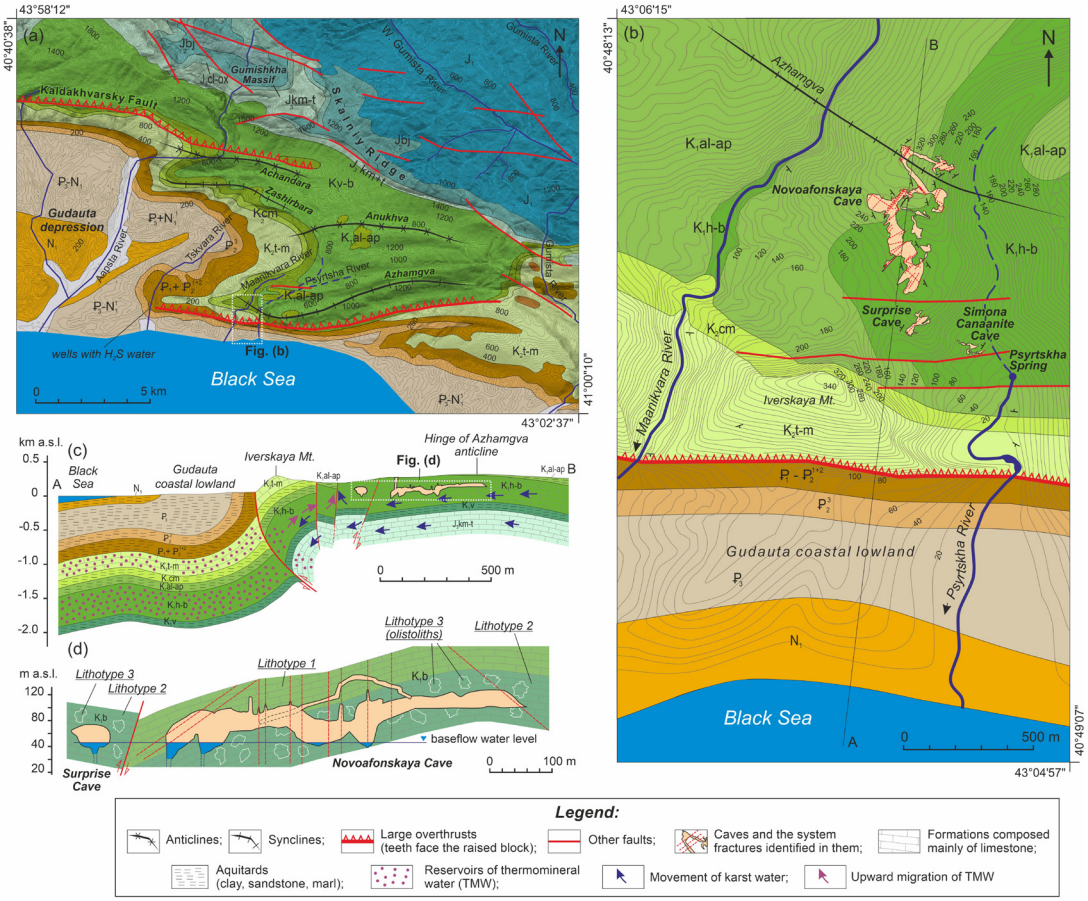

Fig. 2. Geological and hydrogeological conditions of Novoafonskaya Cave: (a) Overview geological map (by Kurochkin et al., 1959 modified by Gamkrelidze, 1959, Dyakonov et al., 1972, Vakhrushev et al., 2001, Rogozhin et al., 2014; relief by SRTM30: Smith & Sandwell, 1997), (b and c) Geological map of the cave area and section along the A–B line (by Bukiya et al., 1971; modified by Klimenko et al., 1974, Dublyansky, 1980 and observations of the authors), (d) Schematic section through Novoafonskaya and Surprise caves along line C-D on (b). *Stratigraphic subdivisions*: **Neogene**. N_1 – *Miocene*. Clays, sandstones, conglomerates. **Paleogene**. P_3 – *Oligocene*. Gypsiferous clays and sandstones. P_2^3 – *Upper Eocene*. Marls. $P_1 + P_2^{1+2}$ – *Lower, Middle Eocene and Paleocene*. Brecciated limestones and marls. **Upper Cretaceous**. K_2t-m – *Maastrichtian, Campanian, Santonian, Coniacian, and Turonian stages*. Limestones and marly limestones. K_2cm – *Cenomanian*. Clays and sandstones. **Lower Cretaceous**. K_1ap-al – *Albian and Aptian stages*. Clays, marls, marly limestones. K_1h-b – *Barremian and Hauterivian*. Limestones. K_1v – *Valanginian*. Limestones, conglomerates, sandstones. **Upper Jurassic**. J_3km-t – *Tithonian and Kimmeridgian*. Limestones, dolomitized limestones, dolomites. J_3cl+ox – *Callovian and Oxfordian*. Sandstones and clays. **Middle Jurassic**. J_2bj – *Bajocian*. Porphyritic tuffs, porphyrites. **Lower Jurassic**. J_1 – Sandstones, mudstones, clays, and shales.

Hydrogeology

A complex of pressurized thermomineral waters, confined to submerged blocks of the Cretaceous limestone, occurs under the coastal Gudauta lowland at depths of 0.5–2.0 km (Sidorenko, 1970). These waters contain dissolved H_2S, CO_2, CH_4, and N_2 (Belenkiy et al., 1982) and are widespread along the entire Black Sea coast of the Western Caucasus. They are recharged by precipitation on high-mountain massifs, sinking into the deep zone through slow circulation along tectonic faults (Vakhrushev, 2009). There is evidence of upward migration of thermomineral waters along tectonic faults. In particular, their participation is established for the Psyrtskha spring, hydrodynamically connected with the Novoafonskaya cave system. The share of thermomineral water in the spring can reach 20% during the baseflow periods (Dublyansky & Kiknadze, 1984). Natural resurgences of thermomineral waters were described in the middle of the 20th century in the valley of the river Tskvara (1.5 km from the sea coast and 4.8 km west of the cave), as well as at the foot of the Iversky Mountain in the city of Novy Afon (Bukiya et al., 1971).

Currently, Novoafonskaya Cave is fed by cold karst waters. In terms of mineralization (TDS < 0.4 g/L), temperature (T = 10–12°C), and chemical composition

(HCO_3-Ca), these waters are typical of the epigene karst of the Western Caucasus (Vakhrushev et al., 2001) (Fig. 3). The karst water level of the cave responds rapidly to precipitation falling on the surface (Mavlyudov et al., 2022), indicating effective conduit permeability. The aquifer is recharged from low-lying carbonate massifs with altitudes of up to 1000–1200 m (Dublyansky & Kiknadze, 1984, Dublyansky, 2006, Mavlyudov et al., 2022). The absence of recharge from the high-mountain massifs is due to the fact that they are separated from the low-lying massifs by a series of faults, the most significant of which is the Kaldakhvarsky fault (Fig. 2a).

Novoafonskaya Cave

Novoafonskaya Cave is located 1.5 km from the Black Sea shore at the western terminus of the Azhamgva ridge (43.09°N; 40.81°E; Fig. 1b). The massif hosting the cave was formed from Lower Cretaceous (Barremian) limestone and is confined by valleys of the Maanikvara River on the west and the Psyrtskha River on the east. Since 1975, Novoafonskaya has been functioning as a touristic show cave, for which the access tunnel was constructed (Fig. 1b).

The length and volume of Novoafonskaya Cave are 3285 m and ca. 1,006,000 m^3 (Fig. 3) (Tintilozov, 1983). Its natural entrance (220 m a.s.l.) is a system of shafts and horizontal chambers with narrow passages, connecting with the main cave in the northeastern part of the Anakopiya Hall. The halls of the southern part of the cave (Anakopiya, Mahadzhirov, and Nartaa) are located at altitudes of 36–90 m a.s.l. The latter represent nearly isometric cavities with a vaulted ceiling up to 35 m high and a total volume of ca. 500,000 m^3.

In the southern halls of the cave, karst waters of the phreatic zone are present as three permanent underground lakes. The siphon conduits of these lakes have been surveyed by divers to a depth of 26 m relative to their baseflow level (Dublyansky, 2006). During the low flow season, the lake level is at 36 m a.s.l. During heavy precipitation events, it could naturally rise to 72–75 m a.s.l., flooding the lower part of the Mahadzhirov Hall. To avoid flooding of the touristic excursion paths, a drainage tunnel was constructed in 1983 to divert flood waters into the Maanikvara River valley (Fig. 1c). Since the construction of the tunnel, lake level fluctuations do not exceed 15 m.

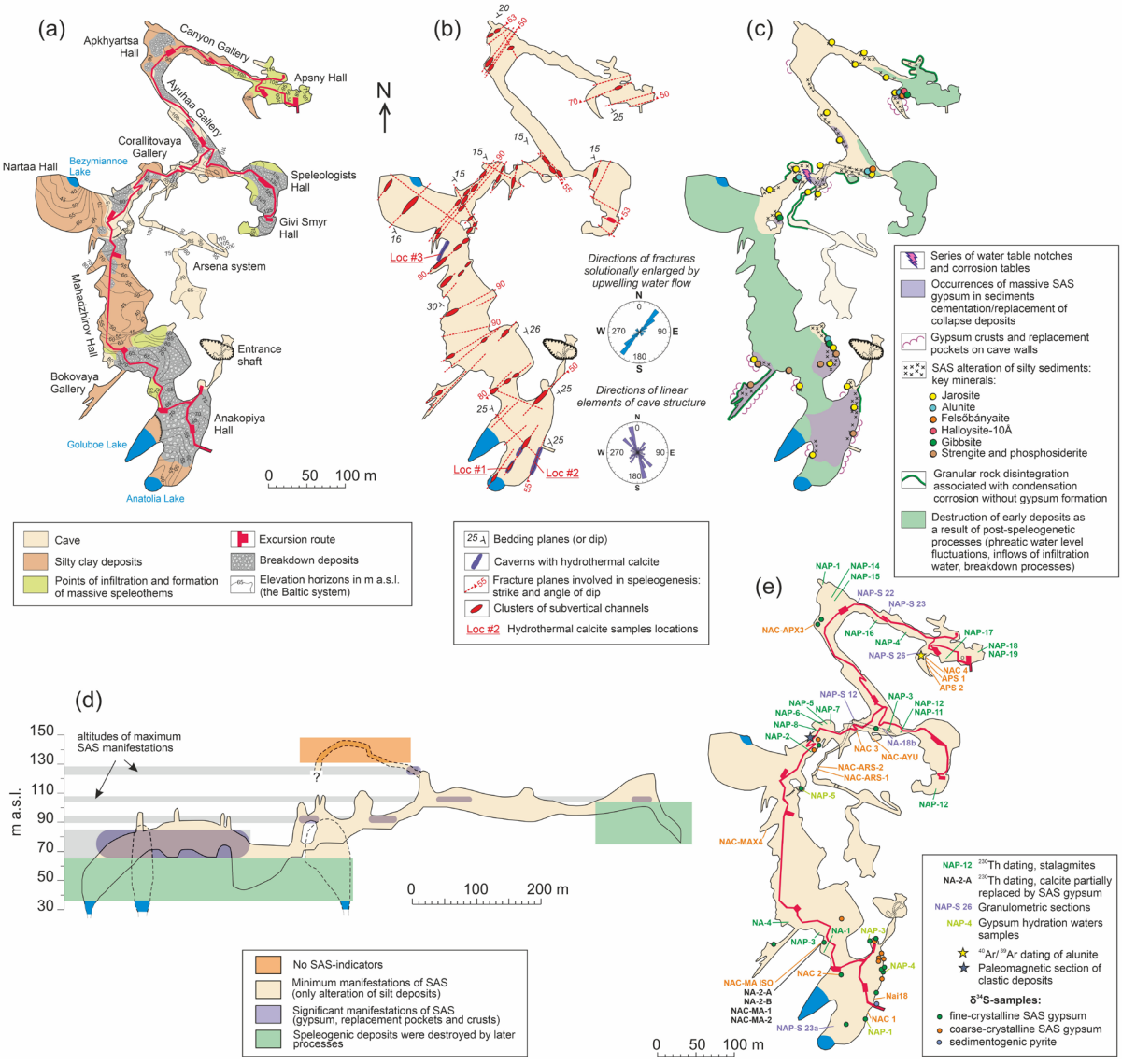

Fig. 3. Structure of Novoafonskaya Cave, speleogenetic indicators, and post-speleogenetic changes: (a) Physiographic map of the cave; (b) Relics of cavities of the early hydrothermal stage and transmissive elements of the massif involved in the main karstification stage; (c) Manifestations of the SAS stage and subsequent (post-speleogenetic) changes; (d) Zones of maximum SAS activity on the vertical profile of the cave; (e) Sampling locations.

The main cavities of the northern part of the cave are located at altitudes of 85–110 m a.s.l. These are mostly linearly extended galleries of NE, NW and SE strike up to 30–40 m wide and 10–30 m high, with several widenings (Apkhyartsa and Apsny Halls). At the south end of Ayuhaa Gallery, there is an eastern branch leading to the system of Speleologist and Givi Smyr halls, located at altitudes of 120–155 m a.s.l. These are among the most voluminous (~200,000 m^3) and highest (up to 75 m) halls in the cave. However, their primary solutional morphology has been completely altered by rockfall processes. The Arsena system (370 m long, at altitudes of 60–150 m a.s.l.) is a series of narrow fissure galleries, shafts and isometric chambers.

Several smaller karst caves exist within the same massif of Novoafonskaya Cave (Fig. 1c). Surprise Cave (length 220 m, volume ca. 43,000 m^3) was encountered during the construction of the access tunnel of the Novoafonskaya Cave. The entrance to the Simon Canaanite cave (160 m long, 2,700 m^3) is located on the right slope of the Psyrtskha River valley. The Maanikvara (190 m long, amplitude 88 m) and Helictitovaya (89 m long, amplitude 35 m) caves are also known (Tintilozov, 1983). In the valley of the Psyrtskha river, which bounds the massif from the east, the Psyrtskha karst spring emerges at an altitude of ca. 32 m a.s.l. with a discharge of 0.7 to 5.0 m^3/s (Ekba & Dbar, 2007). According to the results of the dye tracing, it is hydrodynamically connected with Novoafonskaya Cave (Tintilozov, 1983).

STUDY DESIGN AND METHODS

Geology and hydrogeology studies

The background geological and hydrogeological information reported in earlier publications (Dublyansky, 1980; Tintilozov, 1983; Dublyansky & Kiknadze, 1984) has been updated here by re-examining the field relationships of rock units, orientations of faults and fractures, as well as a focused study of the lithology of cave host rock (petrographic observations) and its stable-isotope geochemistry (O and C). Karst waters of the cave-along with surface, karst, and thermomineral waters of the wider region—were collected in 2016–2020 (along with T and pH measurements) and analyzed for their hydrochemical, stable-isotope ($\delta^{18}O$ and $\delta^{2}H$), and dissolved gas compositions. An expanded discussion of analytical techniques is available in Supplementary section S1.

Cave studies

Morphological observations and documentation of characteristic hypogene karst features was carried out using the guidelines and criteria presented in Klimchouk (2007), Dublyansky (2013), De Waele and Gutiérrez (2022), and De Waele et al. (2024). To constrain the dynamics of paleoflow, a grain-size analysis was performed on fossil and modern fluvial sediments.

Mineralogical and geochemical studies

For morphologies consistent with a hypogene origin, analysis of isotopic alteration of cave walls (O and C) was performed as per Dublyansky et al. (2014), Spötl et al. (2021; 2023). To constrain temperatures of paleo fluids, euhedral crystals of calcite found in some cavities were subjected to fluid inclusion microthermometry and further analyzed for $\delta^{18}O$ and $\delta^{13}C$.

To identify possible manifestations of sulfuric acid speleogenesis (SAS), we searched for minerals indicative of this process (Polyak & Provencio, 2001, Galdenzi & Maruoka, 2003, D'Angeli et al., 2018) in the fine-grained sediments by means of combined scanning electron microscopy – energy dispersive spectroscopy (SEM-EDS) and X-ray diffractometry (XRD) techniques. Gypsum was analyzed for the stable-isotope composition of sulfur ($\delta^{34}S$) and of the hydration water ($\delta^{18}O$ and $\delta^{2}H$).

Chronological constraints on the various stages of speleogenesis were obtained by means of $^{40}Ar/^{39}Ar$ dating of alunite form the SAS-altered sediments, ^{230}Th-U dating of subaerial speleothems (stalagmites, flowstone), and paleomagnetic studies of fossil fluvial sediments (see Supplementary section S1 for expanded discussion).

RESULTS AND INTERPRETATIONS

Lithology and isotopic composition (O and C) of the cave host rock

Anakopiya and Makhadzhirov halls of the southern part of the cave were formed in thickly layered siliceous, locally marly limestone (lithotype 1). The skeletal part of the limestone is composed of algal detritus (bafflestone) encrusted with silica. The rock often contains large (up to several tens of cm) chert nodules alongside inclusions of pyrite and apatite. The northern part of the cave is carved in calcarenite (lithotype 2), comprised of carbonate fragments of fine-sand size (90–500 μm), with a relatively high degree of rounding. Intraclasts as well as rare fragments of faunal remains are tightly packed (grainstone) and cemented by clear-crystalline calcite (intrasparite). Rare detrital grains consist of quartz and K-feldspar. Within this sequence, olistolites of bioclastic limestones with block sizes from 1 to several tens of meters (lithotype 3) are common. Limestone of lithotype 1 is characterized by a significant content of SiO_2 (up to 22.1 mol. %), whereas lithotypes 2 and 3 are near purity (mean $CaCO_3$ = 97.5 and 97.2 mol. %). None of the studied lithotypes contained the sedimentary evaporites hypothesized by Tintilozov (1983). Detailed documentation of lithotypes is presented in Supplementary section S2 and Fig. S1.

The carbonate lithologies of Novoafonskaya Cave are characterized by $\delta^{13}C$ values from +1.4 to +3.5‰ (mean +2.7 ± 0.6‰ VPDB) and $\delta^{18}O$ values from -7.5 to -2.8‰ (mean -4.7 ±1.0‰ VPDB) (n = 537; Supplementary section S2, Fig. S2). The $\delta^{18}O$ of diagenetic veinlets, as a rule, is significantly lower than the limestone matrix (-9.5 to -6.5‰), whereas $\delta^{13}C$ generally does not differ from that of the matrix. The $\delta^{13}C$ of lithotype 1 (+1.4 to +1.9‰) is close to characteristic values of pelagic carbonates from the Barremian of the western Tethys (+1.9 to +2.5‰; Weissert et al., 1985; Sprovieri et al., 2006; Godet et al., 2024), whereas the $\delta^{13}C$ of lithotypes

2 and 3 (+3.1 to +3.3‰) is somewhat higher. The $\delta^{18}O$ of carbonates in all cores analyzed (-7.5 to -2.8‰) is significantly lower than characteristic values of pelagic Tethys carbonates (for Barremian, $\delta^{18}O$ = -3.8 to -1.1‰; Sprovieri et al., 2006).

Hydrogeology of the cave and cave area

Studies in the 1980's (Dublyansky & Kiknadze, 1984) established that the Novoafonskaya Cave presently has no thermal water recharge. Thermal waters are discharged in the neighboring Psyrtskha spring, however, which suggests that mixing corrosion may still be active in the massif. To clarify this uncertainty, we conducted a series of observations in 2017–2020 and complemented our analysis with archival hydrochemical data (2004–2017) provided to us by the Institute of Ecology of Abkhazia.

Thermomineral waters were studied from two flowing wells drilled in the 1950's, located 4.8 km west of the cave at the junction of the southern slope of the Azhamgva ridge with the Gudauta lowland. The wells discharge sulfide-methane waters from Upper Cretaceous deposits at a depth of ca. 600 m, and the wellhead temperature is 41–51°C. Waters have a neutral pH (6.9–7.4), Cl-Na and Cl-Na-Ca compositions, with 5.06–6.15 g/L TDS (Fig. 4a). High concentrations of aqueous SO_4^{2-} (0.76–1.37 g/L) and Mg (0.11–0.18 g/L) are observed in well #1, but for well #2 waters, the concentrations do not exceed 0.4 and 0.08 g/L, respectively. Sulfide content ($H_2S + HS^-$) varies between 6.2 and 23.8 mg/L (Table S2).

Monthly monitoring of cave lake water composition (phreatic water, Fig. 2a, 3a) and of Psyrtskha spring was carried out in 2011–2012. One-off sampling was carried out in 2014–2019, including in Surprise Cave (Tables S3, S4). Cave water is characterized by T = 10–11°C, slightly alkaline (pH = 7.4–8.0), and pure HCO_3-Ca composition with 0.16–0.38 g/L TDS (Fig. 4a, Table S3). Such parameters are typical for karst waters of the Western Caucasus (Vakhrushev et al., 2001). Psyrtskha spring waters differ from karst waters by slightly higher temperature (12.0–12.5°C), TDS (0.28–0.45 g/L), and the presence of Cl (0.034–0.116 g/L; Fig. 4a, Table S4). Concentrations of Li, Cu, Zn, Rb, and Sr in Psyrtskha spring water are also significantly higher than in cave waters (Fig. 4b). Notably, this set of metals often represents a typical association for hydrothermal systems (Brondi et al., 1973, Christensen et al., 1983, Nicholson, 1992).

The proportion of thermomineral water in the karst water of the cave was estimated through mixing proportions by Cl and TDS and found to be 1–4% in our series of observations (Fig. 4c). It was reported to increase up to 20% during extremely low-water conditions (Dublyansky & Kiknadze, 1984). Using the average compositions of thermomineral and cold karst waters as end members, the saturation index to calcite (SI_{calc}) as a function of thermomineral water content was calculated using the Mix function in Aqion 8.2.7. These calculations show that the admixture of thermomineral water, even limited to ≤1%, significantly increases the aggressiveness of water, and the maximum effect is achieved at 20% (Fig. 4d). If thermomineral waters contain dissolved gases (CO_2, H_2S), the mixing corrosion effect is further enhanced.

The isotopic compositions of waters were characterized by monitoring data in 2018–2021 (waters of the Psyrtskha cave and spring, once a month) and one-off samples in 2016–2020 (Table S5). Thermomineral waters are characterized by $\delta^{18}O$ from -12.8 to -12.3‰ and $\delta^{2}H$ from -91.0 to -85.0‰, which corresponds to precipitation at altitudes exceeding 2000 m (Fig. 4e), corroborating the high-altitude recharge suggested for Black Sea artesian complexes (Vakhrushev, 2009).

Karst waters of the cave (n = 116) are characterized by $\delta^{18}O$ values from -11.2 to -7.6‰ and $\delta^{2}H$ from -73.1 to -49.5‰. The range of compositions for Psyrtskha spring waters (n = 39) is almost identical to cave waters: $\delta^{18}O$ = -11.1 to -8.6‰ and $\delta^{2}H$ = -72.1 to -53.6‰. This similarity is explained by the predominance of cold karst waters (96–99%) in spring recharge, for which the isotopic compositions are consistent with those of mean annual precipitation values at 400–1000 m elevation (Fig. 4e). However, since the recharge of karst waters in the Western Caucasus is dominated by isotopically light winter precipitation (Zakharov et al., 2018; Wolf et al., 2024), the actual recharge altitudes are likely to be lower.

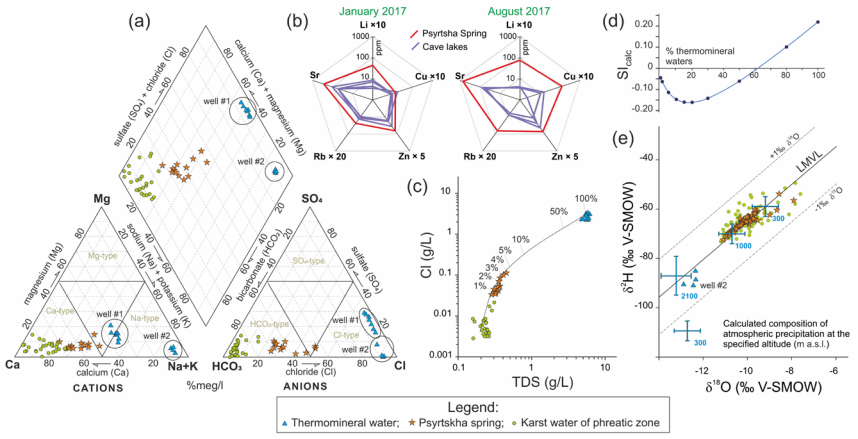

Fig. 4. Hydrogeochemical and isotopic characteristics of groundwater in the cave and immediate area: (a) Thermomineral and karst waters on the Piper diagram; (b) Content of some minor elements in karst waters of the cave and Psyrtskha Spring; (c) Cl and TDS ratios in karst and thermomineral waters with a mixing line for Psyrtskha Spring; (d) Change of saturation to calcite (SI_{calc}) at mixing of cold and thermomineral waters; (e) Isotopic compositions of waters in comparison with mean annual compositions of precipitation at different altitudes (modeled by OIPC; Bowen et al., 2005, error bars 1σ).

Morphological characteristics of speleogenetic stages in Novoafonskaya Cave

Based on observations of the cave morphology, we have identified sets of morphological elements, belonging to the four distinct stages of speleogenesis.

Morphological elements of the early stage (Stage 1)

The earliest solutional cavities, truncated by the cave walls, comprise solution-enlarged fissures and small (up to 15 cm) nearly isometric solutional vugs hosting euhedral crystals of calcite (Fig. S3a). Most of them were observed in halls Anakopiya and Makhadzhirov, in association with SW–NE trending fissures (Fig. 3d). It is noteworthy that the fissures of this orientation were further utilized by fluids of the main speleogenetic stage, indicating the continuity of the fluid-conducting structure.

Morphological elements of the main stage (Stage 2)

The gross morphology of the cave is characterized by a combination of subhorizontal passages (halls and galleries) with clusters of narrow subvertical conduits (entrance shaft, Arsena system). Development of subvertical conduits was most often controlled by SW–NE fractures (Fig. 3b). Near-vertical (80–90°) and inclined (50–55°) fractures prevail, dipping SE and NW. Rift-like conduits (Fig. S3b) alternate with chamber-shaped enlargements at the intersections of bedding planes (Fig. 5b). Meso-morphologies forming as a result of intersection of independently forming cavities (cuspate remnants, pendants, wall niches, arches, bridges, etc.) are common (Fig. S3c). When developing ascending conduits intersected poorly permeable lithological horizons, point feeders and series of discharge cupolas formed (Fig. S3d).

The formation of horizontal cavities was controlled by lateral migration of fluids along bedding planes and networks of intra-bed fractures (Fig. 5c). Conduits with ellipse-shaped cross-sections were formed along strata, and their remnants are preserved as ceiling half-tubes exposed by the collapse of underlying blocks (Fig. 5c, d). Large scallops (sizes of 0.5 to 1 m) were observed on the surface of some half-pipes (Fig. S3f).

Intra- and interstratal fractures were also solutionally widened by upwelling fluids (Fig. 5e). Solutional enlargement of multiple adjacent fractures led to the detachment of large blocks, which collapsed into the cave halls and passages. This mechanism played an important role in shaping the most voluminous halls of the cave: Anakopiya, Makhadzhirov, and Nartaa. The process is evidenced by corrosion forms on the hall's ceilings and walls and solutional morphologies on the surfaces and sides of large collapse blocks residing on the hall's floors.

Fig. 5. Characteristic morphology elements of the Novoafonskaya Cave: (a) Series of ascending channels along parallel cross-cutting fractures; (b) Chambers at intersections with bedding fractures; (c) Phreatic channel following the bedding plane; (d) Ceiling half-pipes; (e) Channels following intra-formation fissures; (f) Signs of declining H_2S water levels: water table notches and corrosion table; (g) Anakopiya Hall, most affected by the SAS; (h) Gypsum replacement crusts; (i) Siliceous nodules from host rocks, "floating" in gypsum replacement crusts; (k) Replacement pockets.

Linear elements of the cave (in plan view; e.g., directions of galleries, contours of hall walls) tend to strike NNW–SSE, NW–SE, and NE–SW. The dominant NNW–SSE strike suggest that the gross cave structure conforms with the hydrodynamic gradient of the karst basin.

Morphological elements of the sulfuric acid speleogenesis (SAS) stage (Stage 3)

Since thermomineral waters of the area contain H_2S, it is expected that karstification by SAS mechanism could have developed during the emergence of the hypogene phreatic system into the vadose zone. Therefore, a focused search for indicators of SAS was undertaken.

Characteristic SAS morphs, including water table notches and corrosion tables, were observed in the Corallite Gallery (Fig. 3c). These forms indicate high aggressiveness at the water-air interface associated with oxidation of H_2S (De Waele et al., 2024). Also observed in the Corallitovaya Gallery and Anakopiya Hall are ceiling pendant drip holes (narrow vertical drip holes with corroded walls in limestone blocks 10–20 cm deep; Fig. S3g), which form by ultra-acidic drip water (Plan et al., 2012).

Morphological elements of the modern stage (Stage 4)

Accessible parts of the cave do not show any morphological features attributable to active modern-day dissolution. While some speleothems exhibit evidence of corrosion in the form of axial holes, this feature is rare, limited to the southern (Anakopiya) and northern (Apsny) halls, and could be a function of locally high and corrosive drip rates. The vadose-zone waters are mostly neutral or slightly supersaturated with respect to calcite, and based on the youngest U/Th ages and successful glass-plate collections of modern calcite, speleothem growth is ongoing today. Conversely, hydrochemical data indicate that dissolution processes are active in the phreatic and epiphreatic zones of the cave.

Settings of the initial thermal stage of speleogenesis

We have reconstructed the initial stage of speleogenesis in Novoafonskaya Cave by studying euhedral calcite crystals (Fig. 3d) deposited in solutional cavities at that time. Crystal diameters can reach 5–10 cm but in most cases do not exceed 2 cm. Calcite $\delta^{18}O$ ranges from -17.9 to -10.1‰, which is significantly lower than the host rock (-7.6 to -3.1‰) and diagenetic calcite (-11.1 to -3.0‰). However, euhedral calcite $\delta^{13}C$ does not differ significantly from either dataset (Fig. 6a).

The variability of $\delta^{18}O$ in euhedral calcite thus suggests fluctuations in paleo-fluid temperatures and parent-water composition, but we also find a relationship with crystal morphology: the lowest $\delta^{18}O$ values were observed for larger, mainly scalenohedral crystals (Fig. 6b). Smaller crystals with complex faceting (scalenohedron and various rhombohedrons and prisms, as well as polycrystals) typically showed higher $\delta^{18}O$ (Fig. 6e). Variations in $\delta^{13}C$ and $\delta^{18}O$ of up to 2–3‰ were observed even within single polycrystals (Fig. 6f).

Several fluid inclusion assemblages (FIAs; Goldstein & Reynolds, 1994) of two-phase inclusions with visually consistent liquid-to-vapor ratios were found in the calcite crystal from Mahadzhirov Hall (Fig. S4). The FIA's yielded homogenization temperatures of 44–48°C, which indicates the involvement of low-temperature thermal waters during the early stage of karstification at Novoafonskaya Cave.

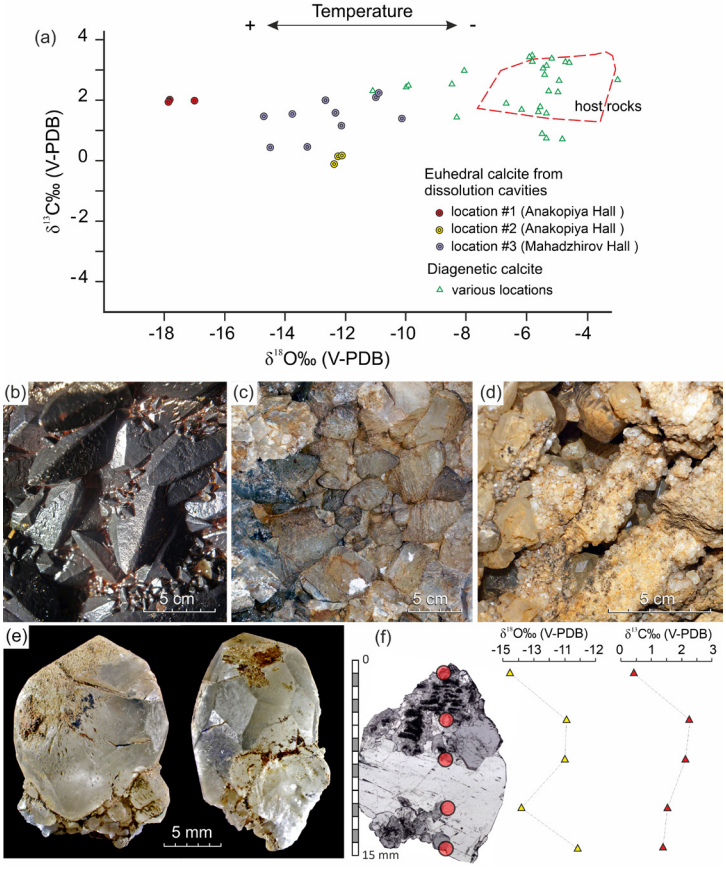

Fig. 6. Euhedral calcite crystals associated with hydrothermal stage: (a) O and C isotopic composition in comparison with host rocks and diagenetic calcite from host rocks (infills of veins, stylolite joints, and micro voids); (b) **Location #1**, scalenohedral crystals (covered with Fe-Mn oxides); (c) **Location #2**, corroded crystals of complex morphology; (d) **Location #3**, dissolution vugs with crystals of various morphologies; (e) Calcite crystals from location #3, showing complex faceting; (f) Section of a polycrystal from location #3 in transmitted light (Nicols partially crossed) and isotopic profiles (red circles).

Settings of the main (phreatic) stage of speleogenesis

To reconstruct the paleo-environments of the main speleogenetic stage (during which the main volume of the cave was formed), we evaluated morphological and sedimentological observations alongside isotopic alteration of wall-rock limestone.

Isotopic alteration of wall-rock limestone

Thirteen 2.5-cm cores ranging from 5 to 22 cm in depth were drilled at representative locations throughout the cave (see Fig 3e for core locations and Fig. S5 for elevations of cores). We specifically tested parts of the cave affected by SAS, as well as dissolution forms related to pre-SAS stages of cave development. Two more cores (SUV-1 and SUV-2) were taken in the Suvenirnaya Cave, located 2.4 km ENE from Novoafonskaya Cave on the northern slope of the Azhamgva ridge (43.108°N 40.838°E; 490 m a.s.l.) (Figs S6, S7). This 11 m long cave is hosted in the same Barremian limestone unit, follows a SE-striking fracture, and has a characteristic hypogene morphology but no evidence of SAS processes.

Cores drilled in the Anakopiya and Makhadzhirov Halls and Corallitovaya Gallery of the Novoafonskaya Cave (Nai18, NAC 1, NAC 2, NAC-MA ISO, NAC-MAX4, NAC 3; Fig 3e) did not show recognizable stable-isotope trends. Four cores (NAC 4, APS 2, NAC-ARS-1 from Novoafonskaya Cave and SUV-2 from Suvenirnaya Cave) demonstrated lower $\delta^{18}O$ values (by 1 to 4‰) and $\delta^{13}C$ values (by 1 to 6 ‰) in the near-cave wall zone (Fig. 7). The coring sites in Novoafonskaya Cave are characterized by a well-preserved phreatic morphology of the main speleogenetic stage and the absence of SAS gypsum. Core SUV-2 was drilled on a wall covered by a crust of translucent palisade calcite (Fig 7e, Fig. S7).

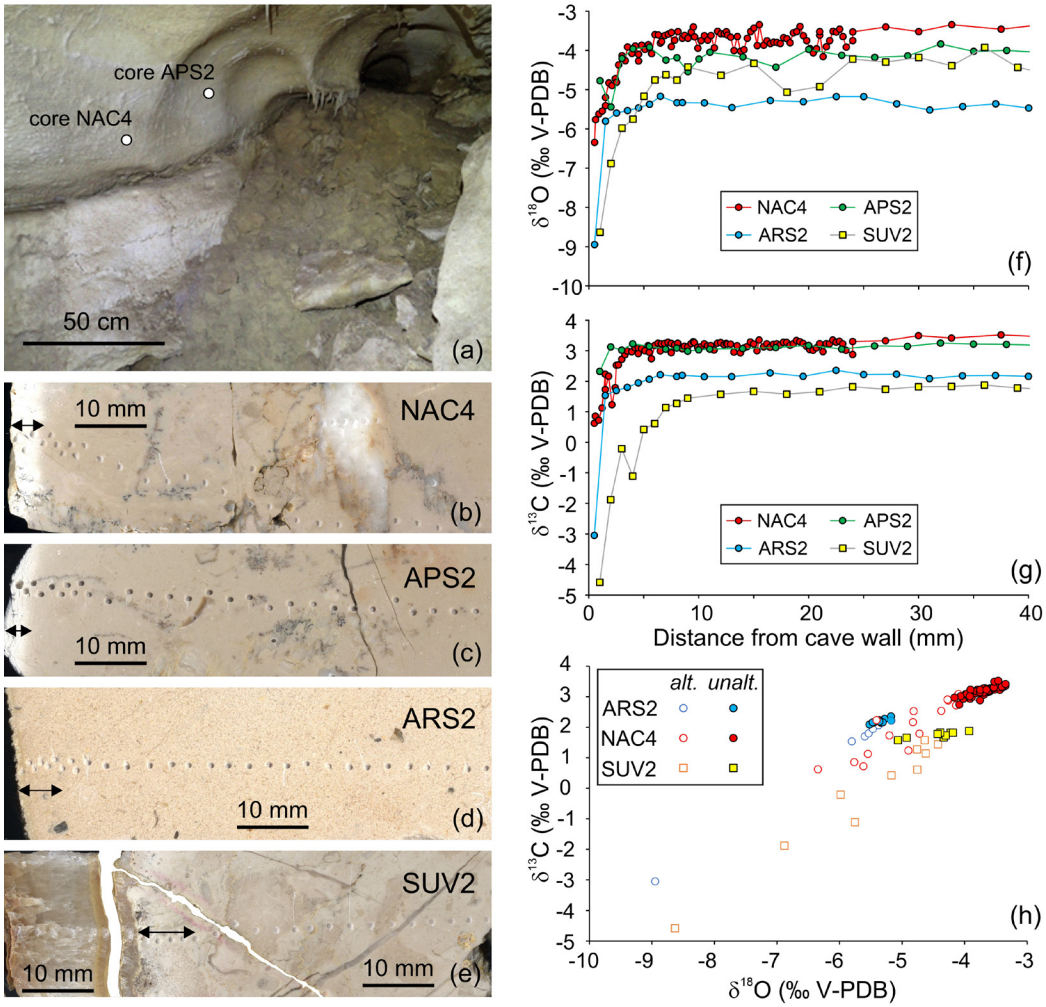

Fig. 7. Isotopic alteration of cave walls: (a) Position of NAC4 and APS2 cores in the phreatic dissolution half-pipe; (b–e) Scans of four cores in which isotopic changes were detected (the double-sided arrow shows the thickness of the altered zone; SUV2 core of calcite deposited on the cave wall (not shown in the isotopic plots); (f and g) O and C isotopic profiles; (h) Isotopic data for altered and unaltered rocks. Cores: NAC4, APS2, ARS2 – Novoafonskaya Cave; SUV2 – Suvenirnaya Cave.

Fluvial cave sediments

To assess paleohydrodynamic conditions, a granulometric analysis of five profiles of intact microfine-grained sediments was carried out (see Fig. 3e for sampling locations and Supplementary section S7 for details). Profile NAP-S 23a represents modern sediments deposited within the zone of modern karst water table fluctuations (39 m a.s.l.). Profiles NAP-2 12, 22, 23, 26 represent fossil sediments deposited at 93–105 m a.s.l.

Sediments are microlayered (less often massive in the lower part of the profile and microlayered in the upper part), dark yellowish orange, yellowish brown and light brown in color. Most of the fossil sediment profiles in the upper part have a 3–30 cm thick zone of secondary alteration. The alteration was caused by the exposure to acidic solutions during the SAS stage (see Section *Associations of authigenic minerals of SAS stage*), which confirms attribution of these

sediments to the main speleogenetic (pre-SAS) stage. Material from alteration zone was not used in the granulometric analysis.

Modern sediments are classified as sandy silt (Fig. 8a) with a predominance of very fine sand, very coarse silt, and coarse silt. Fossil sediments are overall less coarse and classified as silt (55%) and sandy silt (45%), with coarse silt, very coarse silt, medium silt, and fine silt dominating. The clay fraction in modern sediments ranges from 1.1 to 1.4%, while in fossil sediments it ranges from 1.8 to 13.5%.

We estimate that modern sediments were deposited at flow velocities of 0.25–0.5 cm/s (Hjulström diagram, Fig. 8b). Flow velocities during the fossil deposition stage could have been lower, based on their higher clay fraction. The content of fine-grained fractions (clay to fine silt) systematically increases with increasing elevation of the section in the cave; coarse-grained fractions (very coarse silt–medium sand) show the opposite trend (Fig. 8c).

According to XRD data (Fig. S14), the principal minerals in fossil sediments are calcite, quartz, and microcline, which are also typical for modern sediments of the flood zone (Tintilozov, 1983). SEM-EDS revealed pseudomorphs of Fe (oxy)hydroxides by framboidal pyrite in ancient sediments.

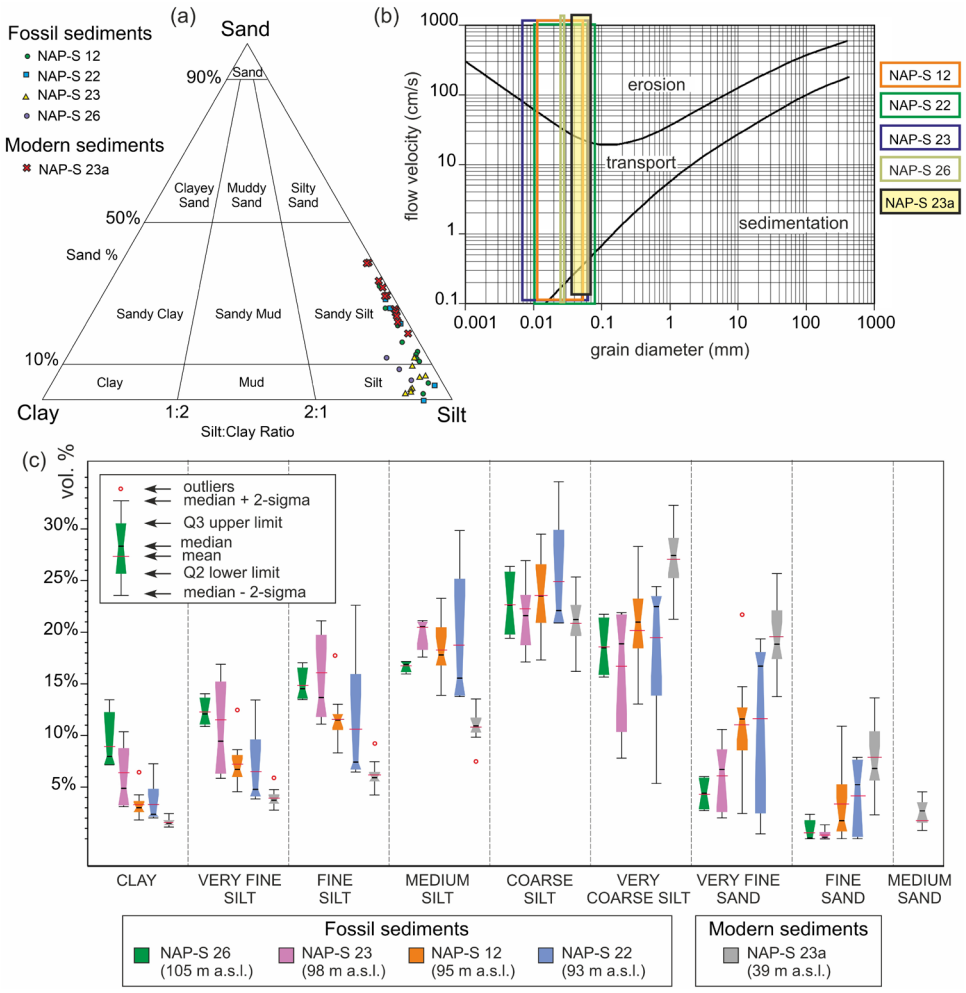

Fig. 8. Granulometric characteristics of modern and fossil sediments of the cave: (a) Position of samples on the discrimination diagram (Folk, 1954); (b) Position of samples on the Hjulström diagram; (c) Grain size of sediments, ranked by height of occurrence in the cave.

Settings of the SAS stage

SAS gypsum deposits

The main product of limestone replacement is gypsum, formed during the reaction of H_2SO_4 with $CaCO_3$ ("SAS-gypsum", "speleogenetic gypsum"; Buck et al. 1994; Galdenzi & Maruoka, 2003). The abundance of gypsum mineralization in the Novoafonskaya Cave was noted from the early stages of its exploration (Dublyansky, 1980; Tintilozov, 1983). In some parts of the cave we encountered white micro-grained gypsum characteristic of SAS (Plan et al., 2012; De Waele et al., 2024) (Fig. 5h-j, Fig. S15a-c). It is composed of subhedral grains up to 30–40 μm in size, sometimes with a secondary evaporitic crust. Deposits of this gypsum type tend to form crusts on cave walls, accumulations on the floors, and breccia cements. Gypsum shows evidence of being formed through metasomatic replacement of limestone, such as faunal pseudomorphs, preserved veinlets, as well as suspended insoluble components of the host limestone, particularly chert nodules (Fig. 5h, i, Fig. S15d).

Crystals and aggregates of gypsum of different morphologies as well as macrocrystalline gypsum crusts (confined to marly limestone varieties) are also found on the cave walls and in loose sediments (Fig. S15e-h). Closely associated with the gypsum development zones are replacement pockets (Fig. 5j) that indicate subaerial corrosion associated with H_2S degassing (Galdenzi & Maruoka, 2003; De Waele et al., 2024). Gypsum replacement and replacement pockets were also observed on the collapse blocks

(and SAS gypsum commonly cements joints between blocks in contact with each other), which confirms their separation near the end of the main (phreatic) stage, in the process of draining the cave (before or during the SAS phase).

The intensity and preservation of SAS traces in the cave are variable. In the lower zone (≤ 67 m a.s.l.) affected by fluctuations of modern karst water table, all traces of former SAS processes (replacement pockets and gypsum) have been removed. Other caves of the massif (Surprise and Simon Canaanite) were also affected by fluctuating water table. The maximum intensity of SAS impact is recorded in Anakopiya and Makhadzhirov Halls at altitudes of 67–85 m a.s.l. (Fig. 3d), where the thickness of replacement crusts reaches 20–30 cm and large replacement pockets are ubiquitous. Weaker manifestations of SAS, appear at altitudes 90–95, 103–108, and 122–130 m a.s.l. (Fig. 3d). Between these elevation intervals, the effect of SAS was limited primarily to shallow (up to a few cm) alteration of siltstone (see Section 4.6.3) and condensation-corrosion not associated with gypsum formation (granular disintegration of limestone, boxwork formation, and other forms of selective corrosion; Fig. S3h). In cavities located above ca. 130 m a.s.l. (e.g., upper part of the Arsena system), features attributable to SAS are absent.

Isotopic characteristics of SAS gypsum and sources of sulfate

Fine-grained SAS gypsum (see Fig. 3e for sample locations) is characterized by $\delta^{34}S$ values from -14.0 to +1.2‰ V-CDT (n = 9). In a 6-cm profile through the gypsum of a replacement pocket from Anakopiya Hall (Fig. 9a, b), $\delta^{34}S$ varied from -14.0 to -7.6‰ (n = 36) with a significant positive trend toward the surface (Mann-Kendall trend test; $p < 0.01$). The $\delta^{34}S$ of macrocrystalline gypsum ranges from -18.3 to -9.4‰ (n = 11), which is significantly lower than microcrystalline SAS gypsum (Kruskal-Wallis test, $p = 0.01$).

Pyrite and marcasite inclusions from reworked sediments of Lower Cretaceous strata (Fig. S16), as well as the SO_4^{2-} and H_2S of modern thermomineral waters, were analyzed to constrain the contribution of different SO_4^{2-} sources. The range of $\delta^{34}S$ in sulfides was -34.9‰ to -14.2 (n = 7), which is lower than most of the microcrystalline gypsum samples studied (Kruskal-Wallis test, $p < 0.01$) but overlaps with the lower range of large gypsum crystals. Conversely, the $\delta^{34}S$ of SO_4^{2-} in modern thermomineral waters (well No. 2 in Primorskoe village, sampled on January 2017) is +22‰, whereas dissolved H_2S has a value of +0.8‰. We discuss enrichment factors and potential mixing of end members in the *Sulfur isotopic composition* section.

Hydration water of SAS gypsum from Anakopiya and Nartaa Halls (n = 4; see Fig. 3e for sample locations) yielded $\delta^{18}O$ values from -12.1 to -9.1‰ V-SMOW and $\delta^{2}H$ values between -115 and -132‰ V-SMOW. Corresponding parent-water values were back calculated using the fractionation factor given by Gázquez et al. (2017): $\delta^{18}O$ = -16.5 to -13.5‰ V-SMOW and $\delta^{2}H$ = -124 to -106‰ V-SMOW (Fig. 9c, Table S7).

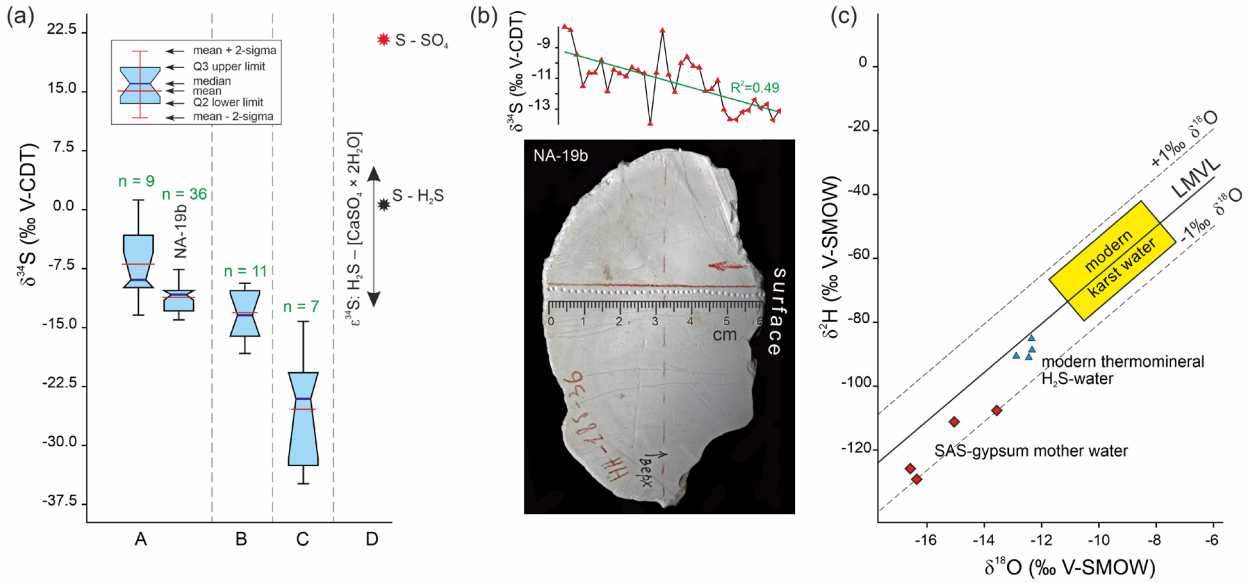

Fig. 9. Isotopic compositions of SAS gypsum ($\delta^{34}S$, $\delta^{18}O$ parent water and $\delta^{2}H$ parent water, ‰), iron sulfides from Lower Cretaceous rocks ($\delta^{34}S$), SO_4^{2-} and H_2S of thermomineral water ($\delta^{34}S$): (a) Range of $\delta^{34}S$ in: A – fine-grained SAS gypsum, B – coarse-crystalline gypsum, C – pyrite and marcasite, D – thermomineral water. $\varepsilon^{34}S$ is shown: H_2S – [$CaSO_4 \cdot 2H_2O$] – range of enrichment factors between oxidation of hydrogen sulfide and precipitation of SAS gypsum (by Hose & Pisarowicz, 1999; Onac et al., 2011; Zerkle et al., 2016; Mansor, 2018); (b) $\delta^{34}S$ profile through SAS gypsum of replacement pocket-gypsum from Anakopiya Hall; (c) isotopic composition of SAS-gypsum parent waters in comparison with modern thermomineral and karst waters.

Associations of authigenic minerals of SAS stage

The thickness of altered layer in fluvial silt sediments varies from a few centimeters in cavities remote from SAS development areas to >2.5 m in Mahadzhirov Hall (Fig. 10a-c). Specific assemblages of authigenic minerals associated with the acid hydrolysis of silicates have been identified in the altered layers (Table 1, Fig. 3c), and the profile exhibits vertical mineralogical zonation (Fig. 10d). The upper part of the section is comprised of fine-grained gypsum and quartz—the latter often represented by euhedral crystals (Fig. 10e). Below this lies a zone of jarosite (Fig. 10f), followed by

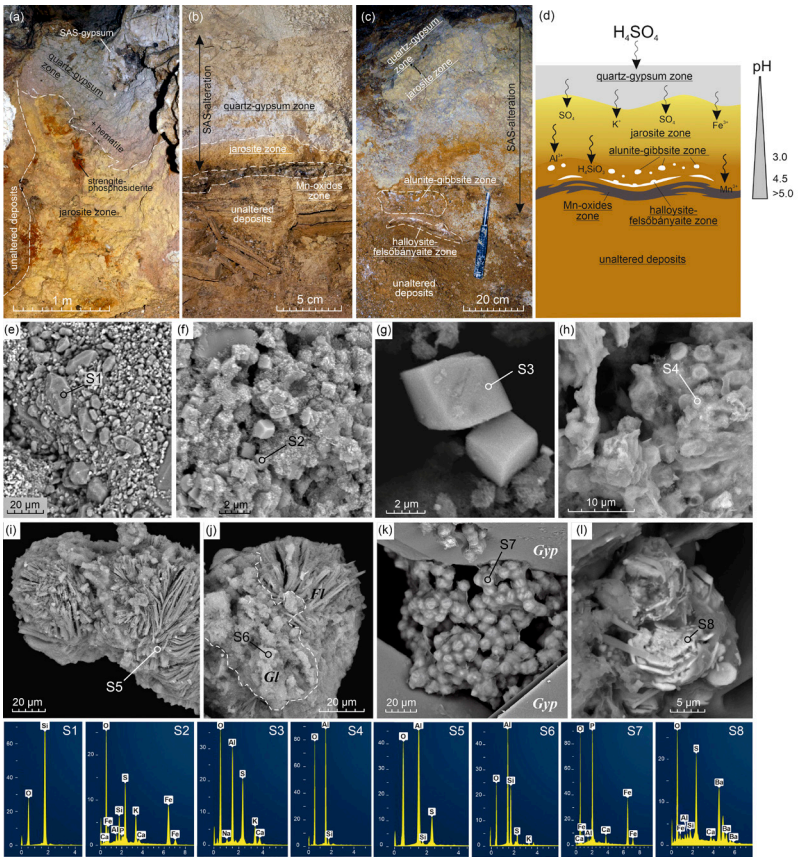

Fig. 10. Distribution of mineral associations in the SAS-altered zone of clastic sediments: (a) Mahadzhirov Hall; (b) Canyon Gallery; (c) Apsny Hall; (d) Conceptual scheme for the formation of vertical mineralogical zonality during decomposition of silicate minerals in siltstones via infiltration of acidic solutions (for more details see Discussion). Key mineral species: (e) euhedral quartz crystals; (f) pseudocubic jarosite crystals; (g) rhombohedral and pseudocubic alunite crystals; (h) collomorphic gibbsite; (i) split crystals of felsőbányaite; (j) halloysite-10Å (Gl), overgrowing felsőbányaite (Fl); (k) spherulites of strengite among gypsum crystals (Gyp); (l) barite crystals. Bottom row images are EDS spectra of the points shown in SEM images.

alunite in association with gibbsite (Fig. 10h), which occurs in milky-white "pockets" below the boundary between these zones (Fig. 10c,d). In the lower part of the profile (Fig. 10c,d), near the contact with the unaltered sediment, interlayers of felsőbányaite and halloysite-10Å occur (Fig. 10i, j). The described vertical zonality is a consequence of the Eh-pH gradient developed in the process of neutralization of acidic solutions upon reactions within the column of silt sediments (see Discussion).

The most common accessory minerals in SAS sediments are strengite in association with phosphosiderite (Fig. 10k, Fig. S17) and barite (Fig. 10l) associated with SAS gypsum. Hematite, goethite, hydroxylapatite and calcite are less common in SAS deposits (Table 1, Figs S17, S18). Hydroxides of Mn (Fig. S18) are characteristic of redox barriers at the interfaces of altered and unaltered substrates.

Table 1. Authigenic minerals of SAS-stage sediments and their distribution in the cave. * An – Anakopiya Hall, Ma – Mahadzhirov Hall, Nar – Nartaa Hall, Kor – Corallitovaya Gallery, Ayu – Ayuhaa Gallery, Ap – Apsny Hall, Ar – Arsen's system (proximal part).

Mineral	Ideal equation (IMA)	Location in the cave*						
		An	Ma	Nar	Kor	Ayu	Ap	Ar
Gypsum	$Ca(SO_4)\cdot 2H_2O$	x	x	x	x	x	x	x
Quartz	SiO_2	x	x	x	x	x	x	x
Jarosite	$KFe^{3+}_3(SO_4)_2(OH)_6$	x	x	x	x	x	x	x
Alunite	$KAl_3(SO_4)_2(OH)_6$		x		x	x	x	
Felsőbányaite	$Al_4(SO_4)(OH)_{10}\cdot 5H_2O$					x	x	
Halloysite-10Å	$Al_2Si_2O_5(OH)_4\cdot 2H_2O$						x	
Gibbsite	$Al(OH)_3$		x	x	x		x	
Hematite	Fe_2O_3		x	x			x	
Goethite	$FeO(OH)$	x	x					x
Hydroxylapatite	$Ca_5(PO_4)_3(OH)$	x						
Strengite	$Fe^{3+}(PO_4)\cdot 2H_2O$	x	x					
Phosphosiderite	$Fe^{3+}(PO_4)\cdot 2H_2O$	x	x					
Barite	$Ba(SO_4)$	x	x		x		x	
Calcite	$CaCO_3$				x	x		

Age constraints of speleogenetic stages

^{230}Th-U ages of speleothems

Two distinct generations of speleothem growth were identified by ^{230}Th-U dating the top and (when practical) bottom of 21 in situ stalagmites (see Fig. 3e for sample locations). The first generation corresponds to MIS 6 and MIS 5 (147.0 ± 1.0 to 88.8 ± 0.4 ka B2K) and occurs only in the northern part of the cave, while the second belongs to MIS 2 and MIS 1 (32.4 ± 0.3 to 0 ka B2K) (see Table S8).

A corroded layered aggregate of pale yellowish orange calcite was found on the western wall of the Mahadzhirov Hall at a height of 68 m a.s.l. The calcite is partially replaced by gypsum, which indicates its formation before the completion of SAS-stage (Fig. 11a). The δ^{13}C ranges from -9.2 to -7.9‰ and δ^{18}O from -14.9 to -14.3‰ (n = 7), consistent with the isotopic composition of glacial-stage stalagmites between MIS 2–6 (Fig. 11b). Four dates have been obtained for this calcite, constraining its age to MIS 6 (170.9 ± 1.8 to 146.9 ± 0.7 ka B2K).

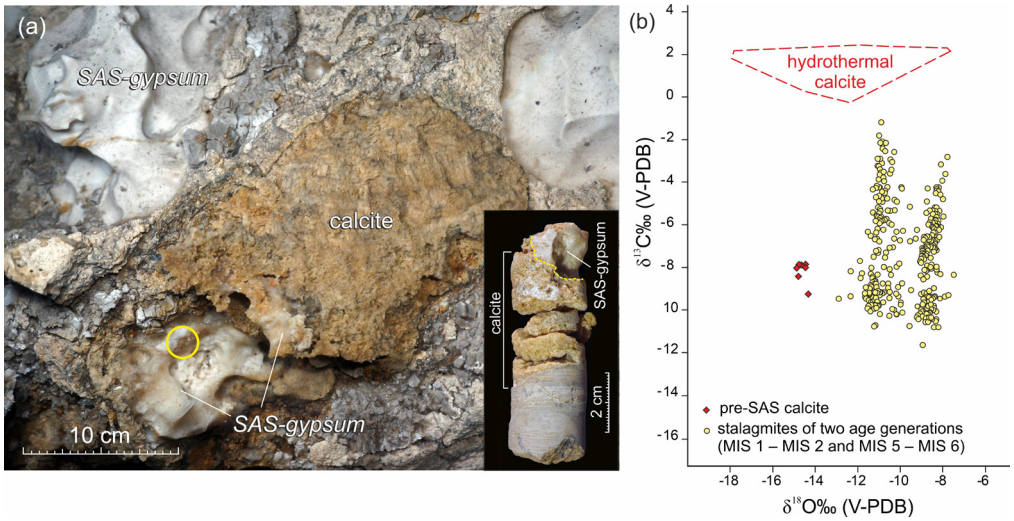

Fig. 11. Speleothemic calcite partially replaced by SAS gypsum: (a) Field photo at coring site; (b) Isotopic composition of C and O.

^{40}Ar/^{39}Ar ages of SAS alunite

An attempt was made to determine the age of alunite sampled from a SAS-altered clayey sediment zone (see Fig.3e for sample positions) using the ^{40}Ar/^{39}Ar method. The alunite was found to be enriched with atmospheric argon, which (coupled with its young age) produced a large uncertainty on the initial ^{40}Ar/^{39}Ar ratio, thereby altering the step heating spectrum in the plateau method to produce a negative age (-0.35 ± 0.15 Ma). Using an isochron method instead yielded a more reasonable age (albeit with large uncertainty) of 1.1 ± 0.4 Ma. Herein, we assume the isochron age for the sediment zone. Despite the uncertainty, this result suggests that the SAS at Novoafonskaya Cave is relatively young, which is generally agreeable with age estimates obtained by other methods.

Paleomagnetic properties of fluivial sediments

Samples for paleomagnetic analysis were collected from an artificial outcrop of subaquatic silty sediments in the Corallitovaya Gallery (see Fig.3e for position; details are available in Supplementary section S9, Fig. S19). The upper part of the 124 cm-thick sequence shows traces of SAS alteration, which confirms that the sediments were deposited during the main speleogenetic (pre-SAS) stage. The most important geochronological constraint from paleomagnetic analysis is that the sediment profile was entirely deposited under normal magnetic polarity, which we assign to the Brunhes normal magnetic polarity chron. Thus, the subaquatic stage is not older than 780 ka in the cavities located above 85 m a.s.l.

DISCUSSION

Preconditions for the development of hypogene karst

A number of factors contributed to the development of hypogene karst in the region of Novoafonskaya Cave. Firstly, the interlayering of limestones with poorly permeable sediments (clay, sandstone, and marl) led to the isolation of aquifers and confined flow conditions. Secondly, the submerged southern limb of the Azhamgva anticline hosts confined thermomineral waters enriched with reactive gases (H_2S and CO_2) that could enhance the aggressiveness of waters via mixing corrosion. Finally, the cave is located near a major tectonic fault and associated smaller faults that provided vertical mobility of water from deeper levels.

Hydrogeological and hydrochemical characteristics of the waters of the Novoafonskaya Cave

In hypogene karst, cold karst and thermomineral waters are often present in the same conduit systems. Due to density differences, they mix only under conditions of forced convection (Audra et al., 2022). Hydrochemical studies indicate that the modern phreatic waters of the cave have no genetic connection with thermomineral waters. Their chemical composition, TDS, and T are typical of cold karst waters of the region. The isotopic and hydrochemical compositions of karst water in the cave are consistent with the recharge on coastal mountain massifs with elevations up to 1200 m (Dublyansky & Kiknadze, 1984; Vakhrushev et al., 2001). At the same time, thermomineral water (few percent up to 20% in

low flow conditions) participates in the recharge of Psyrtskha Spring, which is hydraulically connected with the cave. The calculated saturation indices show that the aggressiveness of water towards calcite increases already at addition of thermomineral water in the amount of 1–4% (as it is most often observed in the Psyrtskha spring). Thus, mixing corrosion is an important speleogenetic mechanism, operating in the massif even presently.

Paleo-environments at various speleogenetic stages

The earliest karstification (Stage 1) in the massif was associated with low-temperature hydrothermal fluids and occurred in closed-system conditions, isolated from biogenic and atmospheric CO_2. Small dissolution caverns hosting large euhedral crystals of calcite (with low $\delta^{18}O$ and high $\delta^{13}C$) formed at this stage. Based on the fluid inclusion thermometry, we constrained the temperature of waters to 44–48°C. The presence of an early hydrothermal stage preceding the main speleogenetic stages is typical for many locations of hypogene karst (Dublyansky, 1990; Spötl et al., 2009; Decker et al., 2018; Temovski et al., 2018).

The $\delta^{18}O$ values of mineral-forming water can be assessed from $\delta^{18}O$ values of calcite and the temperatures of water (assuming crystallization in conditions of equilibrium; Dietzel et al., 2009; Koltai et al., 2024). Using the equilibrium fractionation equation from Coplen (2007), we estimate that paleo water $\delta^{18}O$ ranged between -10.5 and -5.7‰ VSMOW.

The cross-formational fluid-conducting system responsible for the main stage of speleogenesis in Novoafonskaya Cave (Stage 2) is associated with SW–NE striking transverse fractures. These fractures, unrelated to the main tectonic structures (Azhamgva anticline and major faults), also controlled manifestations of ancient hydrothermal karst. Horizontal elements of the cave followed bedding planes and stratabound fractures. At intersections with transverse fractures, enhanced dissolution led to the formation of flattened chambers and passages. Such morphology is diagnostic of mixing corrosion in phreatic conditions.

The morphology of the cave, demonstrating enhanced dissolution at the intersections of vertical fractures and bedding planes, is characteristic of the interaction of ascending cross-formation and lateral interstratal flows. This interaction, involving waters with different chemical properties, activates mixing corrosion and leads to the development of karst caves (Klimchouk et al., 2012, 2017, 2021).

Some phreatic conduits of the cave have large, up to 1 m or more, scallops indicating turbulent flow conditions and flow velocities exceeding 1 cm/s (Curl, 1974; White, 1988). We do not observe morphological signs of density-driven convection, such as Laughöhle cross sections (Kempe et al., 1975, Dublyansky, 2013, Spötl et al., 2023). Large horizontal morphs indicating enhanced lateral enlargement along the water table (Klimchouk, 2007) or thermocline/chemocline (Audra et al., 2022) are also absent.

The particle size distributions of aqueous silty sediments show that they were deposited under sluggish flow conditions (velocities not exceeding 1 cm/s). The main constituents of clastic sediments are calcite, quartz and K-feldspars. These minerals represent the insoluble residue of the host rocks; no minerals attributable to surface provenance were found. Compared to fossil fluvial deposits, their modern counterparts are somewhat coarser grained (Fig. 8c). This suggests quieter hydrodynamic conditions at early stages of cave drainage and higher hydrodynamic gradients at the modern stage.

The sulfuric acid speleogenesis stage (Stage 3) in Novoafonskaya Cave occurred during its emergence from phreatic to vadose conditions. The presence of the SAS stage was diagnosed using the following criteria: (a) morphological indicators of dissolution near and above the H_2S-water table, such as water table notches, replacement pockets, ceiling pendant drip holes; (b) gypsum deposits with metasomatic replacement structures in limestone, yielding low $\delta^{34}S$ (see *Isotopic characteristics of SAS gypsum and sources of sulfate* and *Sulfur isotopic composition sections*); and (c) ubiquitous association with minerals indicative of acid decomposition of silicates and subsequent neutralization of acid solutions (see *Associations of authigenic minerals of SAS stage* and *Isotopic composition of SAS gypsum parent water* sections).

The SAS stage did not leave macro- and meso-morphs characteristic of long-term presence of sulfidic water and condensation-corrosion (Plan et al., 2012; D'Angeli et al., 2019; De Waele et al., 2024). SAS action was limited to mineralogical alteration of the limestone walls of the cave, fine-grained clastic deposits, and the development of micro-morphs (replacement pockets and drip holes). This indicates relatively rapid drainage of a low-dynamic confined aquifer containing thermomineral sulfide waters. The relatively rapid transition of the cave from the phreatic to the vadose state resulted in only insignificant modification of the cave morphology by SAS processes.

Speleogenetic Stages 1 and 2 were previously described in the model of V. Dublyansky (1980), while Stage 3 is distinguished here for the first time. Our morphological and sedimentological observations do not support the contribution of epigene karstification in the origin of the northern parts of the cave (as suggested by Dublyansky, 1980). We found no evidence of dynamic water flows (such as small scallops, erosion potholes, coarse alluvium, etc.) or forms of paragenetic dissolution typical of other epigene caves in the region.

Under current conditions (Stage 4), the phreatic aquifer is well connected to the surface through conduit permeability, as evidenced by the rapid water level response to precipitation (Mavlyudov et al., 2022). Apparently, such an active connection became possible after removal of poorly permeable Albian-Aptian deposits from the karst massifs and their erosional dissection. At present, the cave has all but lost its connection with thermomineral waters. Yet, karstification by mixing corrosion (in its blocks located to the south of the cave) continues in the phreatic zone of the massif at present, as evidenced

by the hydrochemistry data (see *Hydrogeological and hydrochemical characteristics of the waters of the Novoafonskaya Cave* section).

Isotopic composition of host rocks and hypogene alteration

The limestones of Novoafonskaya Cave are characterized by $\delta^{13}C$ values of +1.4 to +3.5‰ and $\delta^{18}O$ values of -7.5 to -2.8‰. The $\delta^{18}O$ values are lower than those of typical Tethys carbonates (Sprovieri et al., 2006), which suggests early diagenetic alteration of the Novoafonskaya Cave host rock by meteoric waters (Swart & Oehlert, 2018).

During the hypogene karstification, water-rock interaction may result in isotopic alteration of the walls of forming cavities. Such changes are diagnostic of hypogene karst and, in some cases, allow estimating the parameters of ancient karst waters (Dublyansky et al., 2014; Spötl et al., 2021, 2023; Temovski et al., 2022). Several cores drilled through characteristic phreatic solutional morphs in Novoafonskaya and Suvenirnaya caves showed conspicuous isotopic alteration. In a 2 to 10 mm-thick rock zone near the cave wall, limestones' $\delta^{18}O$ and $\delta^{13}C$ values are 3 to 7‰ lower than in the bulk rock. The isotopically altered zone also exhibits bleaching. The altered $\delta^{18}O$ values are due to temperature-dependent exchange of O isotopes between water and limestone (Spötl et al., 2021). Change of limestone $\delta^{13}C$ isotope properties in the vicinity of the cave wall is explained by isotopic exchange with dissolved inorganic carbon of the karst water.

Stable-isotope alteration of cave walls was found only in parts of the cave that bear no indications of SAS. No alteration was detected in areas affected by SAS (e.g., Anakopiya and Mahadzhirov Halls). Since SAS is a highly dynamic process (Plan et al., 2012), the rate of cave wall retreat during this process is often faster than the propagation of the alteration front; the latter therefore, has no time to develop. On the other hand, isotopic alteration halos which could have been developed at early hypogene stages are expected to be obliterated by SAS and condensation corrosion processes (Spötl et al., 2021).

Sulfur isotopic composition

SAS-gypsum

The range of gypsum $\delta^{34}S$ in the cave (-14.0 to +1.2‰ V-CDT) is generally characteristic of SAS gypsum (Galdenzi & Maruoka, 2003; Temovski et al., 2018; D'Angeli et al., 2019; 2022; De Waele et al., 2024). Enrichment coefficients ($\varepsilon^{34}S$) between the oxidation of H_2S and precipitation of SAS gypsum lie between -13 and +5‰ (Hose & Pisarowicz, 1999; Onac et al., 2011; Zerkle et al., 2016; Mansor et al., 2018; Temovski et al., 2018). Assuming the present H_2S isotopic composition of thermomineral waters of $\delta^{34}S$ = +0.8‰ (this study), some 73% of gypsum samples fall within the range of possible fractionation via this process. However, the $\delta^{34}S$ of H_2S during the SAS stage could have differed from the present day if there was a change in source or reactive pathways (Seal, 2006).

Lower $\delta^{34}S$ values in larger gypsum crystals may be attributed to contributions from ^{34}S-depleted SO_4^{2-} derived from the oxidation of sulfide minerals in the host rock. Variations in SAS gypsum composition (-14.0 to -7.6 ‰) in a 6-cm profile through the fill of a replacement pocket from Anakopyia Hall reflect the dynamic suite of factors that influenced sulfur isotope fractionation (microbial activity, ventilation, H_2S/O_2) during the SAS (Mansor et al., 2018). Comparable variations of the $\delta^{34}S$ in SAS gypsum have been recorded in other caves (Temovski et al., 2018).

H_2S and SO_4^{2-} of thermomineral waters

The origin of H_2S thermomineral waters from the Black Sea area is a matter of debate, as no marine evaporites are known in the water-bearing Cretaceous rocks. The waters are characterized by low SO_4^{2-} content and high $\delta^{34}S$ in H_2S (+0.8‰). The isotopic composition of SO_4^{2-} ($\delta^{34}S$ = +22‰) is somewhat higher than the $\delta^{34}S$ of Jurassic and Cretaceous sulfates (+17–20‰; Bottrell & Newton, 2006). The absence of SO_4^{2-} and higher $\delta^{34}S$ of H_2S (+8.8 to +11.8‰) is also characteristic of the thermomineral waters in Matsesta spring (Black Sea coast of Sochi, 120 km NW of the cave), which occurs in similar hydrogeological conditions (Pankina, 1966; Posokhov & Tolstikhin, 1977).

High $\delta^{34}S$ in H_2S most often indicates closed-system sulfate reduction under a SO_4^{2-} deficit (consistent with hydrochemical data). When ^{34}S-depleted SO_4^{2-} is disproportionately consumed, the residual H_2S becomes ^{34}S-enriched via a Rayleigh distillation mechanism (Seal, 2006; Wynn et al., 2010). In the absence of massive evaporites (Bukiya et al., 1971; Afanasenkov et al., 2007), potential sources of SO_4^{2-} may be carbonate-associated sulfates, sedimentogenic solutions, and S-bearing bitumen.

Isotopic composition of SAS gypsum parent water

During the crystallization of gypsum, two molecules of water are incorporated in the mineral from the parent solution (hydration water). The $\delta^{18}O$ and $\delta^{2}H$ values of gypsum hydration water reflect the corresponding values for the parent solution. Isotopic fractionation between parent solution and gypsum are practically insensitive to temperature in the range of temperatures of 0–50°C and to salinity below 100 g/L (Gázquez et al., 2017). Thus, the isotopic composition of gypsum hydration water can directly be used to reconstruct that of paleo water in hypogene caves (Gázquez et al., 2022).

The isotopic composition of gypsum hydration water could be altered if the gypsum was exposed for the long time to waters with different isotope composition. Microgranular gypsum is more susceptible to such changes (Gázquez & Hodell, 2022); hence, all samples herein were obtained from dry parts of the cave, not exposed to modern karst waters. Two samples of coarse-crystalline gypsum showed very similar compositions of parent water ($\delta^{18}O$ = -16.3 to -16.5‰ V-SMOW; $\delta^{2}H$ = -121 to -124‰ V-SMOW). Two samples of microgranular SAS gypsum showed a somewhat higher isotopic composition of parent water

($\delta^{18}O$ = -13.5 to -15.0‰ V-SMOW; $\delta^{2}H$ = -106 to -109‰ V-SMOW), which may indicate partial alteration by late fluids. To reconstruct the composition of the paleo-water during deposition of gypsum, we rely on the data obtained from coarse-crystalline gypsum.

The inferred compositions of gypsum parent water are depleted in both ^{18}O and ^{2}H relative to modern-day karst and thermomineral waters. In the context of regional paleoclimate, this may suggest that SAS gypsum was formed during glacial stages of the Late Pleistocene. This is consistent with the speleothem-based proxy record indicating the cold-season temperature control on the $\delta^{18}O$ of meteoric waters in the Black Sea / Western Caucasus region (Wolf et al., 2024). Millennial-scale negative excursions of $\delta^{18}O$ and $\delta^{2}H$ in precipitation around the Black Sea are further attributable to the enhanced delivery of low $\delta^{18}O$ and $\delta^{2}H$ glacial melt waters from the Caspian basin into the Black Sea during deglaciation periods (Badertscher et al., 2011). Because the source of the gypsum parent waters may be associated with deep reservoirs in the restricted circulation zone, transmission time of the meteoric isotopic signal may be exceptionally high but well within the periodicity of orbital dynamics.

Minerogenetic mechanisms of the SAS stage

The association of SAS-stage minerals in Novoafonskaya Cave (gypsum, quartz, jarosite, alunite, gibbsite, halloysite-10 Å, barite, etc.) is typical of other SAS-affected cave systems (Polyak & Provencio, 2001; Onac et al. 2009; Plan et al., 2012; Temovski et al., 2013; Sauro et al., 2014; D'Angeli et al., 2018, 2019; De Waele et al., 2024). Minerals of this association were found in all parts of the cave between 67 and 120 m a.s.l, indicating that most of the cave was exposed to sulfuric-acid solutions to some extent, even in places where SAS gypsum is absent on the cave walls.

Gypsum is the most common SAS-stage mineral in Novoafonskaya Cave and is formed by the reaction of sulfuric acid with the host limestone:

$$CaCO_3 + SO_4^{2-} + 2H^+ + 2H_2O \rightarrow CaSO_4{\cdot}2H_2O + CO_2 + H_2O$$

The greatest variety of mineral species is found in H_2SO_4-altered silt sediments. The mineral associations formed in this process, as well as their vertical zonation in the profile, can be explained by pH gradients interacting with key mineral constituents of the sediment during vertical propagation of the alteration front. As solutions containing H_2SO_4 moved through the sediments, a series of reactions gradually neutralized their acidity and enhanced cation availability. In the upper parts of the alteration profiles, maximum acidity promoted the complete decomposition of silicates. Since the solubility of quartz in acidic conditions is minimal (Bennett et al., 1988), it was deposited in this zone in form of euhedral microcrystals. As the acid solutions became saturated in Al^{3+}, Fe, K^+, and Mn^{2+} due to decomposition of silicates, they became a source of ions for authigenic minerals. The most common mineral of the alunite group is jarosite, which is precipitated at pH < 3 (Brown, 1971; Dill, 2001) and can be formed by the decomposition of microcline:

$$2KAlSi_3O_8 + 2H^+ + 2SO_4^{2-} + 14H_2O + 3Fe^{2+} \rightarrow KFe_3(SO_4)_2(OH)_6 + 6H_4SiO_4 + 2Al^{3+} + K^+$$

The most likely sources of Fe for this reaction are pyrite in the cave sediments, sulfide inclusions in the host rocks, and Fe^{2+} admixtures in marly limestone.

Alunite crystallizes in the range of pH 3.3–4.0 (Sánchez-España et al., 2016), and gibbsite at pH 4.3 and above (Gardner, 1972). The association of alunite and gibbsite, located below the jarosite zone, may be related to the elevated concentrations of Al^{3+} in solutions and pH of 3.3–4.3. Felsőbányaite precipitates from sulfate waters at pH > 4.5 (Lozano et al., 2018), which explains its localization, in association with halloysite-10Å, below the zone of alunite-group minerals at the contact with unaltered sediments.

Barite is common in hypogene karst (Polyak & Provencio, 2001; Sauro et al., 2014; D'Angeli et al., 2018; Galdenzi, 2019; Klimchouk et al., 2021). It is commonly found in accessory amounts in SAS-affected sediments of Novoafonskaya Cave. Deep-seated waters are a typical source of Ba, because it migrates readily in the presence of Cl (Hanor, 2000).

Phosphates in caves are most commonly associated with bat guano (Audra et al., 2019). However, there are no traces of Chiroptera inhabitation at the studied locations in Novoafonskaya Cave. Findings of phosphate within the silty sediment replacement crusts therefore indicate their association with the SAS-alteration stage. Strengite is formed in acidic conditions (pH 2.5-6.0) and a highly oxidizing environment (Figueira et al., 2019), particularly in oxidation zones of sulfide ores (Lindberg & Pecor, 1958). Its presence suggests that the cave was open to the atmosphere during the SAS-alteration stage. Apatite inclusions in the host rock are the most likely source of PO_4^{3-}. Goethite, hematite, and apatite are likely to form late due to remobilization of Fe and PO_4 from jarosite and strengite.

EVOLUTIONARY HISTORY OF THE NOVOAFONSKAYA CAVE

We have presented a comprehensive survey and temporally constrained reconstruction of speleogenetic stages in the fluid-conducting system of Novoafonskaya Cave, which we propose was controlled by the direction and amplitude of tectonic movements, as well as by sea level changes that modulated the base level of karst water drainage. Active formation of fold structures in the Western Caucasus began in the Miocene and continued into the Pliocene (Milanovsky, 1968). This structural setting allowed the development of the cave along SW–NE striking faults, associated with the late stages of the Alpine orogeny in the Miocene (Rastsvetaev et al., 2010). During this time, the priming karstification of Stage 1 took place in deep-seated confined flow conditions (Fig. 12).

Regional karst development was significantly influenced by the Messinian salinity crisis at 5.6–

5.4 Ma, which caused a 500–600 m-drop in water level in the euxinic basin (Popov et al., 2010; Tari et al., 2015; Krezsek et al., 2016). At this time, mature karst systems were formed along the terrain defined by the present-day Black Sea coast and shelf, well below the modern base level (Klimchouk, 2018). Once sea level recovered to near present-day position, the epigene karst caves that formed during the Messinian time could be exploited by deep-seated water flows, similarly to the model proposed for the hypogene karst of South Dobrogea (Lascu et al., 1994).

Faults located along the southern flank of the Azhamgva anticline, formed in association with a series of thrust faults manifested along the entire southern slope of the Greater Caucasus (Rogozhin et al., 2014), served as flow paths for deep waters. Given that these structures date to the late Pliocene (Dyakonov et al., 1972) as a result from subduction of the East Black Sea plate below adjacent areas of the Caucasus (Popkov, 2010), we may conclude that conditions favorable to enhanced deep-seated water flow and development of hypogene karst during Stage 2 occurred between the Late Pliocene and Early Pleistocene (Fig. 12).

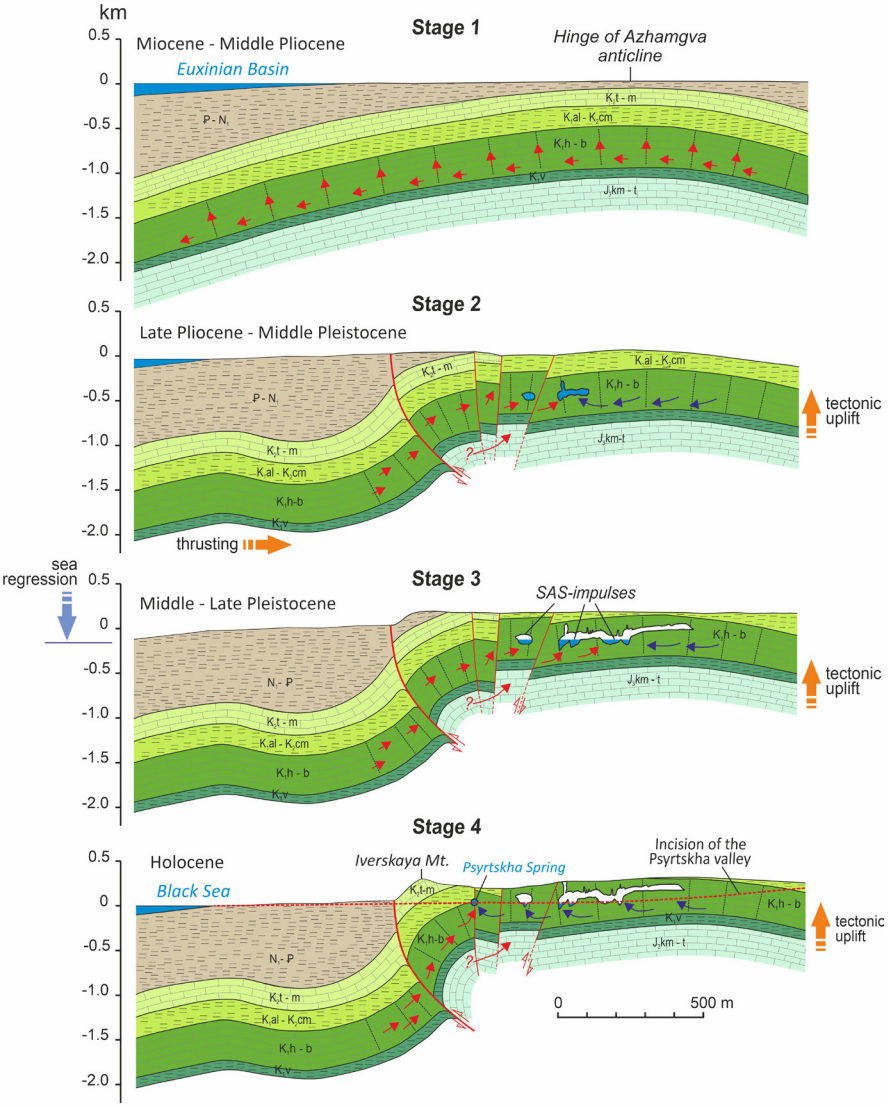

Fig. 12. Conceptual model of speleogenesis of the Novoafonskaya Cave (according to V. Dublyansky, 1980; updated based on the data reported in this paper): **Stage #1:** Early hydrothermal karstification in confined conditions; **Stage #2:** Main speleogenetic stage due to mixing corrosion of thermomineral and cold karst waters; **Stage #3:** Sulfuric acid speleogenesis (SAS) during uplift of the cave into the subaerial zone; **Stage #4:** Modern stage in which the cave is recharged only by cold karst waters, while thermomineral waters emerge south of the cave in the Psyrtskha Spring. Arrow labeled "thrusting" denotes the far-field expression of the East Black Sea plate thrusting below adjacent areas of the Caucasus (Dyakonov et al., 1972; Popkov, 2010).

Tectonic uplift of the Western Caucasus drastically intensified in the Pleistocene. The amplitude of the Greater Caucasus uplift at this time was ca. 300 m for coastal areas and 2000–2500 m for high-mountain massifs (Kogoshvili, 1976). The amplitude of uplift in the coastal massifs of the Western Caucasus can be gauged by the elevations of Early-Chaudinian (550–600 ka, ca. 120 m a.s.l.) and Late-Chaudinian (380–550 ka, ca. 100 m a.s.l.) marine terraces (Milanovsky, 1968; Prutsky, 1999). Since the level of the Black Sea during the Chaudinian times was close to the present day (Svitoch et al., 2000), the elevations of the Chaudinian terraces approximately correspond to the amount of uplift of the coastal massifs over the last ca. 600 ka, which yields an average uplift rate of 0.2 m/ka. The latter estimate, together with the sea level change curve (Svitoch et al., 2000), allows us to assess the change in the position of the cave relative to sea level during the last ca. 600 ka (Fig. 13). Most of the cave resided in the phreatic zone prior to the

end of the Chaudinian transgression, and most of the halls were drained after ca. 400 ka. Since that time, development of SAS above the surface of sulfidic water and the formation of subaerial speleothems (Stage 3) became possible (Fig. 12). The SAS processes were most intensive within a zone immediately above the cave water surface, where conditions for the condensation of water vapor and concentration of sulfuric acid solutions were optimal. The position of this active subaerial SAS zone fluctuated with changing water table levels in the cave. Therefore, both SAS processes and stalagmite growth could take place in the cave simultaneously, albeit in halls of different heights.

Our model is consistent with novel geochronologic constraints obtained in this study. Paleomagnetic data limit the deposition of subaqueous silt in the Corallitovaya Gallery to within the modern epoch of the normal polarity (Brunhes; younger than 780 ka). According to the model (Fig. 13), these sediments must have formed before the end of the Chaudinian transgression (ca. 380 ka), given evidence of SAS alteration that must be associated with lowering of water levels thereafter.

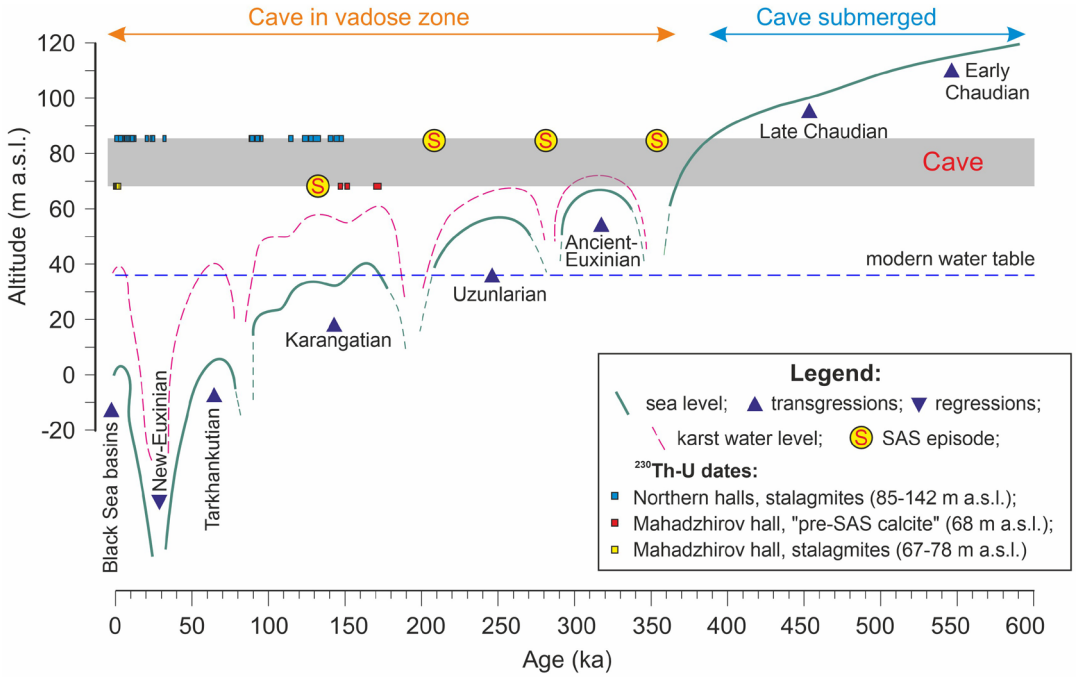

Fig. 13. Chronology of key events in the evolution of the Novoafonskaya Cave: ^{230}Th-U dates of speleothems compared with the Pleistocene Black Sea level curve (Svitoch et al., 2000). Sea levels have been adjusted for the tectonic uplift of the area (their position is shown relative to the cave); a hypothetical curve for karst water level has been added. The gray band is bounded by elevations of 85 m a.s.l. (position of the paleomagnetic section and the oldest dated stalagmites in the Corallitovaya Gallery) and 68 m a.s.l. (position of the oldest dated speleothems in the Mahadzhirov Hall, partially destroyed during the SAS stage = "pre-SAS calcite").

There are no morphological signs of long hiatuses in the cave drainage process, such as deeply incised slit-like notches that form during stationary positions of sulfidic waters. We may infer therefore that either cave drainage was relatively rapid and uniform or that cave waters were not sulfidic during hypothetical pauses in the water table decline.

The age of the youngest speleothems affected by SAS (gypsum replacement) in Mahadzhirov Hall is 147 ka (MIS 6), which constrains the age of the most recent SAS episode to within this interval. In higher elevation halls of the cave, stalagmite growth had already begun by this time, with no signs of SAS processes. The timing of speleothem growth in the upper halls of the cave corresponds to MIS 5-6 and MIS 2-1, whereas the growth of speleothems in the lower part of Mahadzhirov Hall resumed only in the Holocene. In the highest parts of the cave (above 130 m a.s.l.) there are no manifestations of SAS.

At present, the conduits formed in the post-Chaudinian (and possibly earlier) transgressions are used by circulating phreatic waters. The recovery of karst water to near present-day level occurred only in the Holocene, at about 10 ka (Stage 4, Fig. 12).

The following factors contributed to the transition of the cave into its present state and the loss of connection with thermo-mineral water: (a) Continued tectonic uplift, with the catchment areas more distant from the Black Sea rising faster, which leads to increased hydrodynamic gradients in the area of discharge; (b) Denudational removal of poorly permeable sediments of Albian-Aptian age, causing an increase in infiltration recharge of karst waters; and (c) Holocene climate favorable for the development of epigene karst.

ACKNOWLEDGEMENTS

The authors dedicate this paper to the memory of the late Alexander Klimchouk (1956—2023), expressing heartfelt appreciation for his unwavering intellectual support throughout this research project and beyond. Additional thanks are due to: M. Chalmaz, B. Pandariya and V. Markholia (Novoafonskaya Cave Excursion Complex, Novy Afon, Abkhazia) for access to the site, organization of logistics and assistance in field research and collection of samples for karst and atmospheric water monitoring; Y. Ekba (Institute

of Ecology, Abkhazian National Academy, Sukhum, Abkhazia) for providing archival data of hydrochemical monitoring; N. Parshina, P. Khvorov, E. Zenovich (South Urals Research Center of Mineralogy and Geoecology, Ural Branch of the Russia Academy of Sciences, Miass, Russia), I. Musabirov (Institute for Metals Superplasticity Problems, Russian Academy of Sciences, Ufa, Russia), L. Kuzmina (Ufa Institute of Biology, Ufa Research Center of the Russian Academy of Sciences) and L. Leonova (Institute of Geology and Geochemistry, Ural Branch of the Russian Academy of Sciences, Ekaterinburg, Russia) for support in laboratory research; A. Demény (Institute of Geological and Geochemical Research, Budapest, Hungary) for performing analysis of hydration water in gypsum samples. A. Degtyarev, D. Kazadaev, S. Kapralov, S. Muslukhov, and E. Pimenova aided in field work. S.M. Sarbu (Emil Racoviță Institute of Speleology, Bucharest, Romania) and S. Galdenzi (Geology Division, School of Science and Technology, University of Camerino, Italy) participated in valuable discussions on the SAS. Paleomagnetic studies were performed in the Shared Facilities Research Center of IPE RAS (Moscow) and supported by Russian Science Foundation Grant #22-27-00453. We are grateful to the reviewers P. Audra, L. Plan, M. Temovski, and one anonymous reviewer for valuable comments and recommendations that improved the quality of the manuscript.

Authorship statement: OC designed the study, wrote and reviewed the manuscript with contributions from all co-authors; OC, SP, JB, DG, ST, and RD participated in field work; SP and OC performed mineralogical analyses; JB performed ^{230}Th-U dating and stable-isotope analysis (C, O) of speleothems and reviewed the manuscript; DG conducted palaeomagnetic research, wrote, and reviewed the manuscript; VP prepared samples for ^{40}Ar/^{39}Ar dating; MH performed ^{40}Ar/^{39}Ar- dating; ST acquired the limestone cores and reviewed the manuscript; SS performed stable isotope analyses (S); RD project administration, funding acquisition, performed chemical analyses of water; YD participated in field work, performed stable isotope (C, O, H) and granulometric analyses; wrote, and reviewed the manuscript.

REFERENCES

Afanasenkov, A.P., Nikishin, A.M., Obukhov, A.N., 2007. Geological structure and hydrocarbon potential of the East Black Sea region. Nauchnyj mir, Moscow, 172 p. (in Russian).

Audra, P., Bigot, J.-Y., Laurent, D., Vanara, N., Cailhol, D., Cazenave, G., 2022. Hydrodynamic model for independent cold and thermo-mineral twin springs in a stratified continental karst aquifer, Camou, Arbailles Massif, Pyrénées, France. International Journal of Speleology, 51(2), 81-91. https://doi.org/10.5038/1827-806X.51.2.2413

Audra, P., De Waele, J., Bentaleb, I., Chroňáková, A., Krištůfek, V., D'Angeli, I.M., Carbone, C., Madonia, G., Vattano, M., Scopelliti, G., Cailhol, D., Vanara, N., Temovski, M., Bigot, J.-Y., Nobécourt, J.-C., Galli, E., Rull, F., Sanz-Arranz, A., 2019. Guano-related phosphate-rich minerals in European caves. International Journal of Speleology, 48(1), 75-105 https://doi.org/10.5038/1827-806X.48.1.2252

Badertscher, S., Fleitmann, D., Cheng, H., Edwards, R. L., Göktürk, O.M., Zumbühl, A., Leuenberger, M., Tüysüz, O., 2011. Pleistocene water intrusions from the Mediterranean and Caspian seas into the Black Sea. Nature Geoscience, 4(4), 236-239. https://doi.org/10.1038/ngeo1106

Barashkov, A.S., Barashkova, A.S., Kamenev, I.V., 2021. Features of the bottom parts of the Veryovkina cave. Proceedings of the International Conference III Crimean Karstology Readings. Theory and practice of modern karstology and speleology. Simferopol, 106-110 (in Russian).

Belenkiy, S.M., Lavreshkina, G.P., Dulneva, N., 1982. Mineral water. Legkaya i pishchevaya promyshlennost', Moscow, 144 p. (in Russian).

Bennett, P.C., Melcer, M.E., Siegel, D.I., Hassett, J.P., 1988. The dissolution of quartz in dilute aqueous solutions of organic acids at 25°C. Geochimica et Cosmochimica Acta, 52, 1521-1530. https://doi.org/10.1016/0016-7037(88)90222-0

Bottrell, S.H., Newton, R.J., 2006. Reconstruction of changes in global sulfur cycling from marine sulfate isotopes. Earth-Science Reviews, 75, 59-83. https://doi.org/10.1016/j.earscirev.2005.10.004

Bowen G. J., Wassenaar L. I., Hobson K. A., 2005. Global application of stable hydrogen and oxygen isotopes to wildlife forensics. Oecologia, 143, 337-348. https://doi.org/doi:10.1007/s00442-004-1813-y

Brondi, M., Dall'Aglio, M., Vitrani, F., 1973. Lithium as a pathfinder element in the large scale hydrogeochemical exploration for hydrothermal systems. Geothermics, 2(3-4), 142-153.

Brown, J. B., 1971. Jarosite-Goethite Stabilities at 25°C, 1 ATM. Mineralium Deposita, 6, 245-252. https://doi.org/10.1007/BF00208032

Buck, M.J., Ford, D.C., Schwarcz, H.P., 1994. Classification of cave gypsum deposits derived from oxidation of H_2S. In: Sasowsky, I., Palmer, M.V. (Eds.), Breakthroughs in karst geomicrobiology and redox geochemistry. Karst Water Institute, Special Publication, 1, p. 5-9.

Bukiya, S.G., Kolosovskaya, O.V., Abamelik, E.M., 1971. Geological map and map of mineral resources of the Abkhaz Autonomous Soviet Socialist Republic, scale 1: 50.000, explanatory note. Nedra, Moscow, 337 p. (in Russian)

Christensen, O.D., Capuano, R.A., Moore, J.N., 1983. Trace-element distribution in an active hydrothermal system, Roosevelt hot springs thermal area, Utah. Journal of Volcanology and Geothermal Research, 16(1-2), 99-129. https://doi.org/10.1016/0377-0273(83)90086-0

Columbu, A., Audra, P., Gázquez, F., D'Angeli, I., Bigot, J.Y., Koltai, G., Chiesa, R., Yu, T.L., Hu, H.M., Shen, C.C., Carbone, C., Heresanu, V., Nobécourt, J.-C., De Waele, J., 2021. A hypogenic cave system with late-stage condensation-corrosion and epigenic overprinting (Toirano, Liguria, Italy). Geomorphology, 376, 107561 https://doi.org/10.1016/j.geomorph.2020.107561

Coplen, T.B., 2007. Calibration of the calcite-water oxygen-isotope geothermometer at Devils Hole, Nevada, a natural laboratory. Geochimica et Cosmochimica Acta, 71(16), 3948-3957. https://doi.org/10.1016/j.gca.2007.05.028

Curl, R.L., 1974. Deducing flow velocity in cave conduits from scallops. National Speleological Society Bulletin, 36 (2), 1-5.

D'Angeli, I.M., Carbone, C., Nagostinis, M., Parise, M., Vattano, M., Madonia, G., De Waele, J., 2018. New insights on secondary minerals from Italian sulfuric acid caves. International Journal of Speleology, 47(3), 271-291. https://doi.org/10.5038/1827-806X.47.3.2175

D'Angeli, I.M., Parise, M., Vattano, M., Madonia, G., Galdenzi, S., De Waele, J., 2019. Sulfuric acid caves of Italy. A review. Geomorphology, 333, 105-122. https://doi.org/10.1016/j.geomorph.2019.02.025

D'Angeli, I.M., Bernasconi, S.M., Carbone, C., Parise, M., Madonia, G., Vattano, M., De Waele, J., 2022. Sulphur stable isotope signatures from sulphuric acid caves of Italy. Proceedings of the 18th International Congress of Speleology, 4, 185-188.

De Waele, J., D'Angeli, I. M., Audra, P., Plan, L., Palmer, A.N., 2024. Sulfuric acid caves of the world: A review. Earth-Science Reviews, 250, 104693. https://doi.org/10.1016/j.earscirev.2024.104693

De Waele, J., Gutiérrez, F., 2022. Karst hydrogeology, geomorphology and caves. Wiley, Chichester, 888 p. https://doi.org/10.1002/9781119605379

Decker, D.D., Polyak, V.J., Asmerom, Y., 2018. Spar caves as fossil hydrothermal systems: Timing and origin of ore deposits in the Delaware Basin and Guadalupe Mountains, New Mexico and Texas, USA. International Journal of Speleology, 47(3), 263-270 https://doi.org/10.5038/1827-806X.47.3.2173

Dietzel, M., Tang, J., Leis, A., Köhler, S. J. 2009. Oxygen isotopic fractionation during inorganic calcite precipitation – Effects of temperature, precipitation rate and pH. Chemical Geology, 268, 107–115. https://doi.org/10.1016/j.chemgeo.2009.07.015

Dill, H.G., 2001. The geology of aluminium phosphates and sulphates of alunite group minerals: a review. Earth-Science Reviews, 53, 35-93. https://doi.org/10.1016/S0012-8252(00)00035-0

Dublyansky, V.N., 1980. Hydrothermal karst in Alpine folded belt of southern part of USSR. Kras i Speleologia, 3, 18 -38.

Dublyansky, V.N., 1981. Hydrothermokarst caves in the south of the USSR. Peshchery (Caves). Interuniversity collection of scientific papers. Perm State University, Perm', 16-25. (in Russian).

Dublyansky, V.N., 2006. Caves and my life. Perm State University, Perm', 257 p. (in Russian).

Dublyansky, V.N., Kiknadze, T.Z., 1984. Hydrogeology of karst in the Alpine folded region of the USSR. Nauka, Moscow, 127 p. (in Russian).

Dublyansky, Y.V., 1990. Patterns of formation and modeling of hydrothermokarst. Nauka. Sibirskoe otdelenie, Novosibirsk, 151 p. (in Russian).

Dublyansky, Y.V., 2013. Karstification by geothermal waters. In: Shroder, J. (Ed. in Chief), Treatise on geomorphology. Academic Press, San Diego, vol. 6, 57-71. https://doi.org/10.1016/B978-0-12-374739-6.00110- X

Dublyansky, Y.V., Klimchouk, A.B., Spötl, C., Timokhina, E.I., Amelichev, G.N., 2014. Isotope wallrock alteration associated with hypogene karst of the Crimean Piedmont, Ukraine. Chemical Geology, 377, 31-44 https://doi.org/10.1016/j.chemgeo.2014.04.003

Dyakonov, A.I., Tsagareli, A.L., Malovitsky, Y.P., 1972. Tectonic map of the western part of the Caucasus and the adjacent Black Sea (explanatory note). All-Union Scientific Research Institute of Mineral Raw Materials, Moscow, 115 p. (in Russian).

Ekba, Y.A., Akhsalba, A.K., 2018. Physical ecology of the atmosphere (statistics and thermodynamics of the atmosphere, physics of formation, precipitation regime, chemical composition and radioactivity of atmospheric precipitation on the territory of Abkhazia). Akademkniga, Suhum, 431 p. (in Russian).

Ekba, Y.A., Dbar, R.S., 2007. Ecological climatology and natural landscapes of Abkhazia. Papirus-M-Dizajn, Sochi, 324 p. (in Russian).

Figueira, R.L., Horbe, A.M.C., Aragón, F.F.H., Gonçalves, D.F., 2019. Exotic sulphate and phosphate speleothems in caves from eastern Amazonia (Carajás, Brazil): Crystallographic and chemical insights. Journal of South American Earth Sciences, 90, 412-422. https://doi.org/10.1016/j.jsames.2018.12.007

Folk, R.L., 1954. The distinction between grain size and mineral composition in sedimentary-rock nomenclature. Journal of Geology, 62, 344-359. https://doi.org/10.1086/626171

Galdenzi S., 2019. Barite replacement boxwork in the Frasassi caves (Italy). International Journal of Speleology, 48(3), 305-310. https://doi.org/10.5038/1827-806X.48.3.2223

Galdenzi, S., Maruoka, T., 2003. Gypsum deposits in the Frasassi Caves, Central Italy. Journal of Cave and Karst Studies, 65(2), 111-125.

Gamkrelidze, P.D., 1959. Some features of the location of tectonic zones of the folded system of the southern slope of the Greater Caucasus. Proceedings of the Geological Institute of the Academy of Sciences of the GSSR, Tbilisi, 391-396. (in Russian).

Gardner, L.R., 1972. Conditions for direct formation of gibbsite from K-Feldspar – further discussion. American Mineralogist: Journal of Earth and Planetary Materials, 57(1-2), 294-300.

Gázquez, F., Hodell, D.A., 2022. Preservation and modification of the isotopic composition ($^{18}O/^{16}O$ and $^{2}H/^{1}H$) of structurally-bound hydration water of gypsum ($CaSO_4 \cdot 2H_2O$) in aqueous solution. Geochimica et Cosmochimica Acta, 337, 73-81. https://doi.org/10.1016/j.gca.2022.09.042

Gázquez, F., Evans, N.P., Hodell, D.A. 2017. Precise and accurate isotope fractionation factors ($\alpha^{17}O$, $\alpha^{18}O$ and αD) for water and $CaSO_4 \cdot 2H_2O$ (gypsum). Geochimica et Cosmochimica Acta, 198, 259-270. https://doi.org/10.1016/j.gca.2016.11.001

Gázquez, F., Monteserín, A., Obert, C., Münker, C., Fernández-Cortés, Á., Calaforra, J.M., 2022. The absolute age and origin of the giant gypsum Geode of Pulpí (Almería, SE Spain). Geosciences, 12(4), 144. https://doi.org/10.3390/geosciences12040144

Godet, A., Adatte, T., Arnaud-Vanneau, A., Bonvallet, L., De Kaenel, E., Mojon, P.O., 2024. Rise and demise of the Urgonian platform in Switzerland. Geological Society, London, Special Publications, 545(1), SP545-2023. https://doi.org/10.1144/SP545-2023-103

Goldstein, R.H., Reynolds, T.J., 1994. Systematics of fluid inclusions in diagenetic minerals. SEPM Society for Sedimentary Geology, 31, 1-199. https://doi.org/10.2110/scn.94.31

Gusev, A.S., 2018. Hydrology of underground water of Khipsta Massif (Abkhazia). Voprosy geografii, 147, 107-133 (in Russian).

Hanor, J.S., 2000. Barite-celestine geochemistry and environments of formation. Reviews in Mineralogy and Geochemistry, 40(1), 193-275. https://doi.org/10.2138/rmg.2000.40.4

Hose, L.D., Pisarowicz, J.A., 1999. Cueva de Villa Luz, Tabasco, Mexico: reconnaissance study of an active sulfur spring cave and ecosystem. Journal of Cave and Karst Studies, 61, 13-21.

Kempe, S., Brandt, A., Seeger, M., Vladi, F., 1975.

"Facetten" and "Laugdecken", the typical morphological elements of caves developed in standing water. Annales de Spéléologie, 30, 705-708.

Klimchouk, A.B., 2007. Hypogene speleogenesis: hydrogeological and morphogenetic perspecive. Special Paper 1. National Cave and Karst Research Institute, Carlsbad, Special Paper Series, 106 p.

Klimchouk, A.B., 2018. Development of the deepest karst systems and submarine discharge of the Arabika Massif (Western Caucasus): the role of the late Miocene regression of Eastern Paratethys. Geologiya i poleznye iskopaemye Mirovogo okeana, 1, 58-82 (in Russian).

Klimchouk, A.B., Tymokhina, E.I., Amelichev, G.N., 2012. Speleogenetic effects of interaction between deeply derived fracture-conduit flow and intrastratal matrix flow in hypogene karst settings. International Journal of Speleology, 41(2), 161-179. https://dx.doi.org/10.5038/1827-806X.41.2.4

Klimchouk, A.B., Amelichev, G.N., Tymokhina, E.I., Dublyansky, Y., 2017. Hypogene speleogenesis in the Crimean Piedmont, the Crimea Peninsula. In: Klimchouk, A., Palmer, A.N., De Waele, J., Auler, A.S., Audra, P. (Eds.), Hypogene karst regions and caves of the world. Springer, Cham, p. 407-430. https://doi.org/10.1007/978-3-319-53348-3_25

Klimchouk, A.B., Amelichev, G.N., Chervyatsova, O.Y., Tokarev, S.V., Kiseleva, D.V., Potapov, S.S., 2021. Ferruginous accumulations in hypogene karst conduits of Crimean Piedmont: Evidence for a deep iron source for the Kerch-Taman iron-ore province, north Black Sea region. Marine and Petroleum Geology, 127, 104954 https://doi.org/10.1016/j.marpetgeo.2021.104954

Klimenko, V., Kukanov, V., Prokofiev, S., Osipova, T., Prokofiev, S., 1974. Map of the distribution of the main aquifer rock complexes on the territory of Abkhazia. Unpublished report on the topic 13 (16). Adler branch of the Research Institute for Engineering Surveys in Construction of the USSR State Construction Committee (in Russian).

Kogoshvili, L.V. 1976. On the development of the neotectogenic relief of Georgia. Metsniereba, Tbilisi, 307 p. (in Russian).

Koltai, G., Kluge, T., Krüger, Y., Spötl, C., Audra, P., Honiat, C., Leél-Őssy, S., Dublyansky, Y. 2024. Geothermometry of calcite spar at 10–50°C. Scientific Reports, 14, 1553. https://doi.org/10.1038/s41598-024-51937-4

Krezsek, C., Schleder, Z., Bega, Z., Ionescu, G., Tari, G., 2016. The Messinian sea-level fall in the western Black Sea: small or large? Insights from offshore Romania. Petroleum Geoscience, 22(4), 392-399. https://doi.org/10.1144/petgeo2015-093

Kurochkin, V.I., Astakhov, N.E., Chikhelidze, S.S. Sorokina, M.D., 1959. Geological map of the USSR. Caucasian series. Leaf K-37-XI. Scale 1:200.000. State Scientific and Technical Publishing House of Literature on Geology and Subsoil Protection, Moscow (in Russian).

Lascu, C., Popa, R., Sarbu, S.M., 1994. Le karst de Movile (Dobrogea de Sud). Revue Roumaine de Géographie, 38, 85-94.

Lindberg, M.L., Pecor, W.T. 1958. Phosphate minerals from the Sapucaia Pegmatite Mine, Minas Gerais. Boletim da sociedade brasileira de geologia, 7(2), 5-15.

Lozano, A., Fernández-Martínez, A., Ayora, C., Poulain, A., 2018. Local structure and ageing of basaluminite at different pH values and sulphate concentrations. Chemical Geology, 496, 25-33. https://doi.org/10.1016/j.chemgeo.2018.08.002

Mansor, M., Harouaka, K., Gonzales, M.S., Macalady, J.L., Fantle, M.S., 2018. Transport-induced spatial patterns of sulfur isotopes ($\delta^{34}S$) as biosignatures. Astrobiology, 18(1), 59-72. https://doi.org/10.1089/ast.2017.1650

Mavlyudov, B., Kuderina, T., Grabenko, E., Kudikov, A., Ekba, Y., 2022. Some data about lakes of Novoafonskaya Cave, Caucasus, Republic of Abkhazia. Proceedings of the 18th International Congress of Speleology, 3, 45-48.

Milanovsky, E.E., 1968. Recent tectonics of the Caucasus. Nedra, Moscow, 483 p. (in Russian).

Nesmeyanov, S. A., 2012. Suture zones as upper crustal seismogenic structures. Geoekologiya, 1, 3–26 (in Russian).

Nicholson, K., 1992. Contrasting mineralogical-geochemical signatures of manganese oxides: guides to metallogenesis. Economic Geology, 87, 1253-1264. http://dx.doi.org/10.2113/gsecongeo.87.5.1253

Onac, B.P., Sumrall, J., Tămaş, T., Povară, I., Kerns, J., Dârmiceanu, V., Vereş, D. Lascu, C., 2009. The relationship between cave minerals and H_2S-rich thermal waters along the Cerna Valley (SW Romania). Acta Carsologica, 38, 27-39.

Onac, B.P., Wynn, J.G., Sumrall, J.B., 2011. Tracing the sources of cave sulfates: a unique case from Cerna Valley, Romania. Chemical Geology, 288, 105-114. https://doi.org/10.1016/j.chemgeo.2011.07.006

Pankina, R.G., Mekhtieva, V.L., Grinenko, V.A., Churmanteeva, M.N., 1966. Isotopic composition of sulfur sulfates and sulfides in waters of some areas of the Ciscaucasia in connection with their genesis. Geokhimiya, 9, 1087-1094 (in Russian).

Peel, M.C., Finlayson, B.L., McMahon, T.A., 2007. Updated world map of the Köppen-Geiger climate classification. Hydrology and earth system sciences, 11(5), 1633-1644. https://doi.org/10.5194/hess-11-1633-2007

Plan, L., Tschegg, C., De Waele, J., Spötl, C., 2012. Corrosion morphology and cave wall alteration in an Alpine sulfuric acid cave (Kraushöhle, Austria). Geomorphology, 169-170, 45-54. https://doi.org/10.1016/j.geomorph.2012.04.006

Polyak, V.J., Provencio, P., 2001. By-product materials related to H2S-H2SO4 influenced speleogenesis of Carlsbad, Lechuguilla, and other caves of the Guadalupe Mountains, New Mexico. Journal of Cave and Karst Studies, 63 (1), 23-32.

Popkov, V.I., 2010. Structural geology of the junction zone of the Black Sea basin and the Caucasus. Geologiya. Izvestiya Otdeleniya nauk o Zemle i prirodnyx resursov Akademii nauk Bashkortostana, 15, 21-28 (in Russian).

Popov, S.V., Antipov, M.P., Zastrozhnov, A.S., Kurina, E.E., Pinchuk, T.N., 2010. Sea level fluctuations on the northern shelf of the Eastern Paratethys in the Oligocene-Neogene. Stratigrafiya. Geologicheskaya korrelyatsiya, 18(2), 99-124 (in Russian).

Posokhov, E.V., Tolstikhin, N.I., 1977. Mineral water. Nedra, Leningrad, 240 p. (in Russian).

Prutsky, N.I. (Ed.), 1999. Explanatory note to the geological map K-37-IV. Caucasian Series, Scale 1:200.000. GNC FGUGP Yuzhmorgeology, FGUGP Kavkazgeolsemka (in Russian).

Rastsvetaev, L.M., Marinin, A.V., Tveritinova, T.Y., 2010. Late Alpine disjunctive systems and geodynamics of the Western Caucasus. Fizika Zemli, 5, 31-40 (in Russian).

Rogozhin, E.A., Ovsyuchenko, A.N., Lutikov, A.I., Sobisevich, A.L., Sobisevich, L.E., Gorbatikov, A.V., 2014. Endogenous dangers of the Greater Caucasus. O.Y. Schmidt Institute of Physics of the Earth, Moscow, 256 p. (in Russian).

Sánchez-España, J., Yusta, I., Burgos, W. D., 2016. Geochemistry of dissolved aluminum at low pH: hydrobasaluminite formation and interaction with trace metals, silica and microbial cells under anoxic conditions. Chemical Geology, 441, 124-137. https://doi.org/10.1016/j.chemgeo.2016.08.004

Sauro, F., De Waele, J., Onac, B.P., Galli, E., Dublyansky, Y., Baldoni, E., Sanna, L., 2014. Hypogenic speleogenesis in quartzite: the case of Corona 'e sa Craba cave (SW Sardinia, Italy). Geomorphology, 211, 77-88. https://doi.org/10.1016/j.geomorph.2013.12.031

Seal, R.R., 2006. Sulfur isotope geochemistry of sulfide minerals. Reviews in Mineralogy and Geochemistry, 61 (1), 633-677. https://doi.org/10.2138/rmg.2006.61.12

Sidorenko, A.V. (Ed.), 1970. Hydrogeology of the USSR. Volume 10. Georgian SSR. Nedra, Moscow, 404 p. (in Russian).

Smith, W.H.F., Sandwell, D.T., 1997. Global sea floor topography from satellite altimetry and ship depth soundings. Science, 277, 1956-1962. https://doi.org/10.1126/science.277.5334.1956

Spötl, C., Dublyansky, Y., Meyer, M., Mangini, A., 2009. Identifying low-temperature hydrothermal karst and palaeowaters using stable isotopes: a case study from an alpine cave, Entrische Kirche, Austria. International Journal of Earth Sciences, 98, 665-676. https://doi.org/10.1007/s00531-007-0263-2

Spötl, C., Dublyansky, Y., Koltai, G., Honiat, C., Plan, L., Angerer, T., 2021. Stable isotope imprint of hypogene speleogenesis: lessons from Austrian caves. Chemical Geology, 572, 120209. https://doi.org/10.1016/j.chemgeo.2021.120209

Spötl, C., Dublyansky, Y., Koltai, G., Racine, T., Plan, L., 2023. The Obir caves adjacent to the Periadriatic Fault in southern Austria: uplifted hypogene caves formed by carbonic acid speleogenesis. Geomorphology, 441, 108901. https://doi.org/10.1016/j.geomorph.2023.108901

Sprovieri, M., Coccioni, R., Lirer, F., Pelosi, N., Lozar, F., 2006. Orbital tuning of a lower Cretaceous composite record (Maiolica Formation, central Italy). Paleoceanography, 21(4), PA4212. https://doi.org/10.1029/2005PA001224

Svitoch, A.A., Selivanov, A.O., Yanina, T.A., 2000. Paleohydrology of the Black Sea Pleistocene Basins. Water Resources, 27, 594-603. https://doi.org/10.1023/A:1026661801941

Swart, P.K., Oehlert, A.M., 2018. Revised interpretations of stable C and O patterns in carbonate rocks resulting from meteoric diagenesis. Sedimentary Geology, 364, 14-23. https://doi.org/10.1016/j.sedgeo.2017.12.005

Tari, G., Fallah, M., Kosi, W., Floodpage, J., Baur, J., Bati, Z., Sipahioğlu, N.Ö., 2015. Is the impact of the Messinian Salinity Crisis in the Black Sea comparable to that of the Mediterranean? Marine and Petroleum Geology, 66, 135-148. https://doi.org/10.1016/j.marpetgeo.2015.03.021

Temovski, M., Audra, P., Mihevc, A., Spangenberg, J., Polyak, V., McIntosh, W., Bigot, J.-Y., 2013. Hypogenic origin of Provalata Cave, Republic of Macedonia: a distinct case of successive thermal carbonic and sulfuric acid speleogenesis. International Journal of Speleology, 42(3), 235–246. https://doi.org/10.5038/1827-806X.42.3.7

Temovski, M., Futó, I., Túri, M., Palcsu, L., 2018. Sulfur and oxygen isotopes in the gypsum deposits of the Provalata sulfuric acid cave (Macedonia). Geomorphology, 315, 80-90. https://doi.org/10.1016/j.geomorph.2018.05.010

Temovski, M., Rinyu, L., Futó, I., Molnár, K., Túri, M., Demény, A., Otoničar, B., Dublyansky, Y., Audra, P., Polyak, V., Asmerom, Y., Palcsu, L., 2022. Combined use of conventional and clumped carbonate stable isotopes to identify hydrothermal isotopic alteration in cave walls. Scientific Reports, 12(1), 9202. https://doi.org/10.1038/s41598-022-12929-4

Tintilozov, Z.K., 1976. Karst caves of Georgia. Metsniereba, Tbilisi, 275 p. (in Russian).

Tintilozov, Z.K., 1983. Novoafonskaya cave system. Metsniereba, Tbilisi, 151 p. (in Russian).

Vakhrushev, B.A., 2009. Peculiar features of hypogene speleogenesis in the folded mountain region of the Western Caucasus. In: Klimchouk, A.B., Ford, D.C. (Eds.), Hypogene speleogenesis and karst hydrogeology of artesian basins. Ukrainian Institute of Speleology and Karstology, Special Paper 1, 271-274.

Vakhrushev, B.A., Dublyansky, V.N., Amelichev, G.N., 2001. Karst of the Bzyb Ridge, Western Caucasus. Publishing of RUDN University, Moscow, 164 p. (in Russian).

Weissert, H.J., McKenzie, J.A., Channell, J.E.T., 1985. Natural variations in the carbon cycle during the Early Cretaceous. The carbon cycle and atmospheric CO_2: natural variations Archean to Present, 32, 531-545 https://doi.org/10.1029/GM032p0531

White, W.B., 1988. Geomorphology and hydrology of karst terrains. Oxford University Press, New York, 480 p. https://digitalcommons.usf.edu/kip_articles/2160

Wolf, A., Baker, J.L., Tjallingii, R., Cai, Y., Osinzev, A., Antonosyan, M., Amano, N., Johnson, K.R., Skiba, V., McCormack, J., Kwiecien, O., Chervyatsova, O.Y., Dublyansky, Y.V., Dbar, R.S., Cheng, H., Breitenbach, S.F.M., 2024. Western Caucasus regional hydroclimate controlled by cold-season temperature variability since the Last Glacial Maximum. Communications Earth & Environment, 5, 66. https://doi.org/10.1038/s43247-023-01151-3

Wynn, J.G., Sumrall, J.B., Onac, B.P., 2010. Sulfur isotopic composition and the source of dissolved sulfur species in thermo-mineral springs of the Cerna Valley, Romania. Chemical Geology, 271(1-2), 31-43. https://doi.org/10.1016/j.chemgeo.2009.12.009

Zakharov, E.V., Kimber, V.B., Rezvan, V.D., Tokarev, I.V., Mavlyudov, B.R., 2018. Results of isotopic investigations in 2013–2016 on karst areas of Sochinskiy speleological region (Western Caucasus) (in Russian). Voprosy geografii, 147, 57-87 (in Russian).

Zerkle, A.L., Jones, D.S., Farquhar, J., Macalady, J.L., 2016. Sulfur isotope values in the sulfidic Frasassi cave system, central Italy: A case study of a chemolithotrophic S-based ecosystem. Geochimica et Cosmochimica Acta, 173, 373-386. https://doi.org/10.1016/j.gca.2015.10.028